Memoirs of the Faculty of Engineering, Nagoya University
Vol. 28, No. 2. (1976)

COMPRESSION OF METALS AND EFFECTS OF PRESSURE ON DEFECTIVE LATTICE

HISAO MII, IKUYA FUJISHIRO and MASAFUMI SENOO

Department of Mechanical Engineering

(received October 29, 1976)

CONTENTS

General Introduction 192
I Pressure Calibration Based on the NaCl Internal Standard 194
1. 1. Introduction 194
1. 2. Experimental apparatus 195
1. 2. 1. X-ray press 195
1. 2. 2. Pressure cell 195
1. 3. Experimental procedures 196
1. 4. Results 197
1. 4. 1. Bi_{III-V}, Sn_{I-II} and $Fe_{\alpha-\varepsilon}$ transformation pressures 197
1. 4. 2. $Pb_{fcc-hcp}$ transformation pressure 198
1. 5. Discussions 198
1. 5. 1. Comparison of the present results with those of recent measurements 198
1. 5. 2. Error estimation 200
1. 6. Conclusion 200
II Pressure Effects on Phase Diagram of Al-rich Al-Si Alloys 201
2. 1. Introduction 201
2. 2. Experimental 201
2. 2. 1. High pressure apparatus 201
2. 2. 2. Pressure cell and samples 202
2. 2. 3. Experimental procedures 204
2. 3. Results and discussions 204
2. 3. 1. Temperature dependence of electric resistance 204
2. 3. 2. Solubility limit of Si in Al 207
2. 3. 3. Quenching of samples 209
2. 3. 4. High pressure phase diagram 211
2. 4. Conclusion 212
III Pressure Effects on Atomic Vacancies of Platinum 212
3. 1. Introduction 212
3. 2. Experimental 213
3. 2. 1. Experimental apparatus and high pressure cell 213
3. 2. 2. Measurements of electrical resistance 215
3. 2. 3. Quenching 215
3. 3. Results and discussions 216

3. 3. 1. Cooling rate of quenching 216
3. 3. 2. Quenched-in resistivity increment 217
3. 3. 3. Boron Nitride as quenching medium 219
3. 4. Conclusion 219
Ⅳ Measurements of Lattice Compression by High Pressure X-ray Diffractometry 220
4. 1. Introduction 220
4. 2. Experimental apparatus and procedures 220
4. 2. 1. High pressure apparatus and X-ray diffractometer 220
4. 2. 2. Sample and pressure cell 222
4. 2. 3. Experimental procedures 223
4. 2. 4. Error correction 224
4. 2. 4. 1. Correction of error due to off-centering of sample 224
4. 2. 4. 2. Correction of error due to the truncation of the diffracted Debye cone 226
4. 3. Results and discussions 227
4. 3. 1. Lattice compression 227
4. 3. 1. 1. Aluminum 227
4. 3. 1. 2. Silicon 229
4. 3. 2. Accuracy 230
4. 3. 3. Correction of the peak shifts due to stacking faults 232
4. 3. 4. Correction on Bridgman's pressure scale 233
4. 4. Conclusion 234

General Introduction

"Pressure" is one of the most important variables of state in the thermodynamics of the matters, nevertheless by far it was less interested than the "temperature" in the material studies.

With the G. E.'s great achievement of synthesising man-made diamond in 1955 as a momentum, a movement to make use of the pressure positively for the studies of meterials seems to had ruled that time in the world-wide scale. Also our country was not made an exception of such trend having now almost twenty years' research history of the field of high pressure sciences.

Even in our laboratory in the Faculty of Engineering, Nagoya University, fifteen years have elapsed since the high pressure metal studies had been undertaken.

In this period study set about most early in our laboratory was a series of researches on the pressure standards. Since to assign a generating pressure an exact value had been the most basic important item of the study, here and there many had engaged in the high pressure calibration works. However, there had been a significant discrepancies among the announced pressure values of the calibrant metals. In the light of such a situation, we devoted ourselves to the pressure calibration works for years. Then we employed thoroughly the NaCl internal standard method along with the D. L. Decker's NaCl scale as the experimental technique. With a combination of the sample metal as the calibrant, the x-ray press (WC-opposed anvil press equipped with x-ray diffractometer), the equipment for measuring electrical resistance and NaCl as the internal standard material, we have determined values of the

pressure-induced transformations of metals tested. These were Bi, Sn, Fe and Pb which should act as the pressure standard in such a very high level as 70 to 150 kbar. Although the details will be extended later, the present values were much lower than the approved reference pressure values. We contended long to reduce the then approved pressure values by 5 to 20 kbar in the same level, but owing to the revisions made later our values now have been conformed well to the most recent reference pressure standards.

Another field of study set about in the earliest stage was the research on the high pressure phase diagram of an Al-Si alloy, in whcih especially we took aim at the effects of pressure on the solid solubility of the solute (Si) in the solvent metal (Al). With the combination of a girdle-type press, the electrical resistance measurement and the micro-photographical observation of the quenched samples, we first determined at 28 kbar the solid solubility of Si in the Al-rich side of the Al-Si alloy. Of course the composition-temperature phase diagram was made in the same alloy, showing that the pressure has enlarged significantly the solid solution range and also enhanced very much the melting point of Al and the eutectic temperature of the alloy.

It was a matchless opportunity to promote our various research plans that in 1973 two of the cubic anvil press whose edge is 6 mm and 15 mm respectively had been installed along with the strong rotary target type x-ray source, 60 kV and 200 mA, in our high pressure laboratory. We lost no time in continuing the phase diagram study. With the combination of the 15 mm cubic anvil press, the electrical resistance measurement and the x-ray diffractometrical analysis of the solid-quenched samples, the solubility limit of Si had been determined much more precisely at a higher pressure 54 kbar. The corresponding composition-temperature phase diagram has been also obtained.

One of the research subjects we had long been interested in was the effect of pressure on the behavior of the atomic vacancies in a metal. Atomic vacancies exist in a metal lattice as the defects thermodynamically in equilibrium with the pertaining temperature and pressure. It is conceived that the vacancies play important roles on the physical and mechanical properties of the metal through the such processes as diffusion and aging. To study the behavior of the atomic vacancies there had been a pertinent method in which a metal concerned was quenched from a high temperature to a low one. By this quenching the excess atomic vacancies generated in that metal at high temperature would be frozen to low temperature which could be measured as the incremental electrical resistance. However, almost all of the quenching experiments put into practice so far were the works under ordinary pressure. Since the experiment would be made particularly harder under high pressure, only few were performed under gas pressure of about 6 kbar. We developed a quenching method of metal in which a solid pressure transmitting medium for generating very high pressure was available again for the solid cooling medium of the quenching. Thus the freezing of vacancies was extended to such a very high level as 60 kbar for Pt. By means of the measurements of the electrical resistance the temperature and pressure dependence of the vacancy concentration was also obtained, and lastly the formation enthalpy, the formation volume of a vacancy and the lattice relaxation around a vacancy have been deduced.

The pressure dependence of the volume of a solid offers an important information for the discussions of the thermodynamical stability under very high pressure. With a combination of the 6 mm cubic anvil press, the strong x-ray diffractometer and

the NaCl internal standard as the pressure calibrant, several pressure-volume relationships have been determined precisely up to such a high level of 100 kbar. It should be announced that in two phases of this study novel improvements have been made. The first one was on the correction of the errors. One error originates in the off-centering of the sample metal in the pressure cell, and another comes from the geometrical truncation of the x-ray optical system employed, both of which are such that inevitable in the high pressure experiments. The second improvement was that hydrostatical compression had been made available in the $6\times6\times6$ mm^3 cell.

The present report describes a few of the experimental results obtained during the progresses of our high pressure metal studies. Our dearest wish is to receive comments which will be the precious moments for the future developments.

Chapter I Pressure Calibration Based on the NaCl Internal Standard[1,2]

1. 1. Introduction

In a high-pressure generator which makes use of a solid material as the pressure-transmitting medium it is hard to determine the magnitude of the generated pressure by means of a primary-type manometer, because of pressure gradients within the pressure cell, and also associated shear and frictional forces between the cell wall and the transmitting medium. This is particularly true where the pressure generator has anvils or a cylinder supported by a gasket. Under these circumstances the pressure-induced transformations of metals and alloys are normally assigned to fixed points of pressure, and these pressure values are calibrated somehow against a primary-type manometer.[3-5]

In the 1968 NBS Symposium[6] the values observed so far for these fixed points up to 100 kbar were carefully considered and were provisionally put forward as the basis for a high-pressure scale up to 100 kbar. However, for the much higher transformation pressures of such metals as iron, barium, and lead the Symposium gave values only for reference. Consequently it is not surprising that there have been large differences between the NBS Symposium scale and the values subsequently observed by various authors (Drickamer[7], Vereshchagin *et al.*[8]).

Another method for determining the pressures in solids, by making use of their P-V relationships (*e. g.* in ionic materials), has become available for pressure generators provided with facilities for X-ray diffraction studies (Jeffery *et al.*[9]). By assigning available values of compressibility and the Grüneisen constant to the energy terms in the Mie-Grüneisen equation of state of NaCl, Decker [10,11] obtained a semiempirical relationship between the pressure and compressibility of NaCl, and published a table of reliable values representing the pressure in NaCl for a given temperature and lattice contraction; this is now known as Decker's scale. By employing new data for the compressibility of NaCl, Decker [12] has recently revised his old scale and published Decker's new scale.

To make the pressure-induced transformation of an element a fixed point of pressure, it should be needed that the observed values of the pertaining transformation originated from different kinds of pressure generator coupled with different principles of observation would converge into a reasonable narrow range of pressure.

With a method based on the NaCl internal-standard technique, we have examined

by X-ray diffraction samples compressed between Bridgman-type anvils in order to determine the transformation pressures of the several pressure-sensitive metals, such as Bi_{III-V}, Sn_{I-II}, $Fe_{\alpha-\varepsilon}$ and $Pb_{fcc-hcp}$. Especially as for the transformation of Pb which should occur at a much higher pressure, Drickamer[7] and Vereshchagin *et al.*[8] have already discussed the location of this transformation by electrical resistance measurements, and Takahashi *et al.*[13] and Mao *et al.*[14] have made direct X-ray diffraction measurement on Pb through diamond anvils. Each has assigned a pressure value to the $Pb_{fcc-hcp}$ transformation, but so far no one has related these transformation pressures to the NaCl scale. Recently Yagi and Akimoto[15] have reconfirmed the transformation pressure of Pb by making use of the cubic anvil X-ray press and the NaCl internal pressure standard.

In the present chapter are described the determinations of the pressure values of the transformations, Bi_{III-V}, Sn_{I-II}, $Fe_{\alpha-\varepsilon}$ and $Pb_{fcc-hcp}$, which are detected by a change in the electrical resistance, made by using the Bridgman-type anvil X-ray press and the NaCl internal pressure standard.

1. 2. Experimental apparatus

1. 2. 1. X-ray press[16]

In Fig. 1 is shown the loading system of the present X-ray press. By a 20-ton hydraulic ram resting on the upper frame of the press force is exerted to press the top one of the opposed WC anvils on to the bottom one. Between the anvil faces the pressure cell is inserted. X-ray is introduced into the pressure cell in the direction perpendicular to the compression axis.

The anvil faces were work-hardened by the pre-pressing up to 100 kbar and ground slightly before service. By this provision the cavity formed on the anvil face during the active pressure was reduced within only 4 microns or the less in depth.

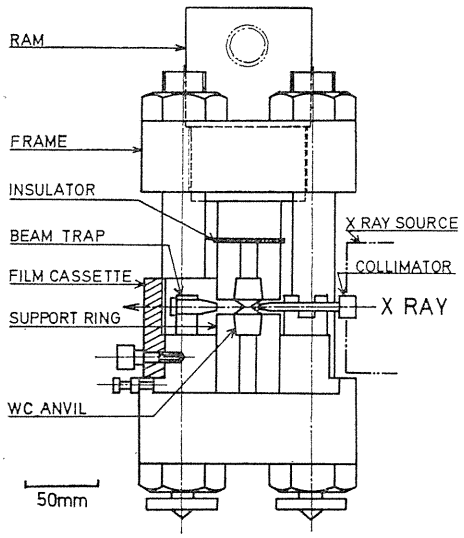

Fig. 1. Opposed anvil press equipped with an X-ray diffraction camera.

1. 2. 2. Pressure cell

It is said that the Bridgman-type anvils are inferior to other pressure generators in its hydrostatical nature within the compressed volume. However, we learned that this problem would be solved by adopting a larger sample cell made of such material as boron having a very small center volume in which enclosed with the calibrant NaCl a pressure-sensitive metal is embedded not to come in touch with the anvil surfaces.

Figure 2 shows the configuration of the sample cell. The pressure-transmitting medium is a disk, 3 mm in diameter and 0.4 mm thick, consisting of a press-formed mixture of 85 wt% amorphous boron powder and 15 wt% epoxy resin. The disk has a centre hole within which an 0.005 mm thick foil specimen, along with silver

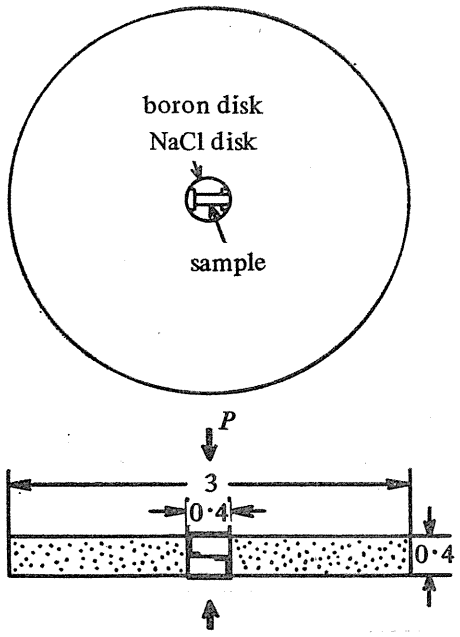

Fig. 2. Configuration of the sample cell for the pressure calibration.

current-conducting foils, is embedded between the plugs, 0.35 mm in diameter and 0.2 mm thick, made from spectroscopic standard grade NaCl. As the pressure-sensitive metal specimens, Bi (six nines), Sn (four nines), Fe (electrolytic iron) and Pb (six nines) were employed.

1. 3. Experimental procedures

The pressure-induced transformation of the specimen was detected by the change of the electrical resistance for both increasing and decreasing pressure cycles. The electrical resistance of the foil specimen was measured by means of a Kelvin double bridge whose potential leads were attached to points very close to the sample cell. This means that the measured electrical resistance includes, in addition to the resistance of the foil specimen, the two contact resistances : that between the specimen and Ag foils and that between the Ag foils and the anvil surfaces. However, since the sum of these contact resistances is estimated not to exceed a few tens of mΩ, these did not interfere with accurate detection of the transformation.

Since the transformation took place abruptly and was completed in a short time in each of Bi and Sn, it was easy to confirm the most probable transformation point Bi_{III-V} or Sn_{I-II}. Although the starting point of the transformation of Fe could be detected by the electrical resistance change, the progress of the transformation was too slow to confirm its completion. Then for Fe the starting point of the transformation was regarded as $Fe_{\alpha-\varepsilon}$. On the other hand it has been reported that the fcc-hcp transformation in Pb at high pressure is very sluggish, having a large hysteresis in pressure. Factors such as overshooting of the loading, variation of stress distribution in the pressure-transmitting medium, deformation of the sample cell, and the phase transformation rate can significantly alter the transformation pressure. In the present experiment on Pb special regard has been paid to give samples sufficient time to transform in a steady condition by a very slow loading.

The pressure was increased at the rate of 1 ~ 5 kbar/h. With these rates it took about 8 ~ 25 days to complete one pressure cycle. The experiments were performed at 25 ℃.

Once the transformation had begun the ram pressure of the press was held constant for some hours to enable a Debye-Scherrer diffraction pattern to be made of the NaCl portions of the sample cell. Zr-filtered Mo-Kα radiation was used at 50 kV and 20 mA, and the diffracted rays were photographed through Al filter, 0.2 mm thick, to prevent fluorescence. An exposure of about 5 ~ 6 h was required to obtain a diffraction pattern.

The diffraction pattern taken at a pressure level was analysed in regard to all or some of those diffractions as (200), (220), (222), (400), (420), and (422), and the arithmetrical average of all the readings was regarded as the lattice constant a_p of NaCl at that pressure. With the lattice constant a_0 of NaCl at the atmospheric pressure the percent compression,

$$(a_p - a_0)/a_0 = -\Delta a/a_0 \tag{1}$$

was calculated for each of the transformations. By applying these NaCl compression data to the Decker's conversion table[12], the corresponding pressure values are obtained.

1. 4. Results

1. 4. 1. Bi_{III-V}, Sn_{I-II} *and* $Fe_{\alpha-\varepsilon}$ *transformation pressures*

Since the transformation took place abruptly and was completed in a short time in each of bismuth and tin, it was easy to confirm the most probable transformation point Bi_{III-V} or Sn_{I-II}. Although the starting point of the transformation of Fe could be detected by the electrical resistance change, the progress of the transformation was too slow to confirm its completion. Then for Fe the starting point of the transformation was regarded as $Fe_{\alpha-\varepsilon}$.

In Table 1 are listed the results of the X-ray diffraction. These transformation pressures, 74±4, 94±4 and 111±4 kbar, are mean values of two or three runs on Bi, Sn and Fe, respectively.

While it is common to represent a pressure-induced transformation with the upstroke pressure value, the downstroke transformation was also detected clearly for each of Bi and Sn. Their percent compression data, the corresponding pressure values and the ranges of hysteresis are shown for reference. As for Fe, however, no data were obtained since the anvil faces were fractured during the downstroke.

Table 1. Transformation pressure of Bi, Sn and Fe.

Metals	Transformation pressure (kbar)		Hysteresis (kbar)
	Upstroke	Downstroke	
Bi_{III-V}	74±4	66±3	8
Sn_{I-II}	94±4	89±5	5
$Fe_{\alpha-\varepsilon}$	111±4		

1.4.2. $Pb_{fcc\text{-}hcp}$ *transformation pressure*

While the starting point of the transformation of $Pb_{fcc\text{-}hcp}$ is distinctly detected, the resistance continued to change slowly for 66 h under constant ram pressure. Even when the resistance value had become almost constant, it still increased, though very slightly, when the ram pressure was raised. The resistance changes observed in one run of the present experiments during the transformation were 17% for the upstroke and 13% for the down stroke. There is a slight difference between the resistance changes observed for each of the runs. This can be attributed to minor differences in the geometrical shape of the cells and in the loading rates used in the runs. To complete the transformation the ram pressure at which the transformation started had to be raised by 10%.

The diffraction pattern of NaCl was taken at a pressure very close to that of the transformation. The point at which the NaCl diffraction pattern was taken is not, strictly speaking, the starting point of the transformation. The small difference, however, was corrected using the relationship between ram pressure and NaCl pressure obtained near the transformation pressure.

The results made on three sample cells are shown in Table 2. During the downstroke, the lead wires of sample cells 1 and 2 were broken; this made the measurements impossible and no data are available for the downstroke in these runs. The table also shows that the pressure value for cell 1 was somewhat higher than those for cells 2 and 3. This can be attributed to the much higher loading rate used in cell 1. The three pressure values obtained give 137 kbar for the loading cycle as the mean with a standard deviation of 3 kbar.

Table 2. Transformation pressure of Pb.

	Transformation Pressure (kbar)	
	Upstroke	Downstrok
Cell 1	143	
Cell 2	134	
Cell 3	135	99
Mean	137±3	

1. 5. Discussions

1. 5. 1. Comparison of the present results with those of recent measurements.

As mentioned before, to assign the pressure-induced transformation of an element

Table 3. Transformation pressures around 100 kbar.

Author	Pressure device	$Bi_{III\text{-}V}$ (kbar)	$Sn_{I\text{-}II}$ (kbar)	$Fe_{\alpha\text{-}\varepsilon}$ (kbar)
Stark et al.[17] (1964)	Opposed anvil	81 ± 4	99 ± 4	118 ± 6
Giardini et al.[18] (1964)	Hexahedral anvil	81 ~ 82		
Jeffery et al.[9] (1970)	Tetrahedral anvil	73.8 ± 1.3	92 ± 3	
Mii et al.[1] (1970)	Opposed anvil	74 ± 4	94 ± 4	111 ± 4

to a fixed value of pressure, measurements from various sources should converge into a reasonable narrow range of pressure. Table 3 will serve to compare the present values with other recent measurements.

(a) Bi_{III-V}

Bi_{III-V} is a transformation which has a lot of data. So far Bi_{III-V} was assigned to high values beyond 80 kbar. In the last ten years, however, values less than 80 kbar were reported from various sources. Although the types of pressure generator differ from each other, the present value agrees very well to that obtained by Jeffery *et al.*[9] using the NaCl internal standard. After that Hall[19] made a correction to the X-ray values of several workers by means of the new Decker's equation of state of NaCl.[12] These are 76 ± 4 kbar (the present value), 75.6 ± 1.3 kbar (Jeffery *et al.*) and 75.0 kbar (Ahlers). Comparing with another value 77.5 ± 1.0 kbar of Kennedy, he stated that agreement was improved now to such a narrow range as 3 %. Thus to assign Bi_{III-V} to a high value beyond 80 kbar seems to be a matter of question in the present time.

(b) Sn_{I-II}

A high value 113-115 kbar had been assigned to the transformation Sn_{I-II}. However, values below 100 kbar appeared recently from two sources. While the value of Jeffery *et al.*[9] is very close to the present one, that of Stark and Jura[17] is rather high. Although more data should be needed to confirm, Sn_{I-II} seems to be around 95 kbar.

(c) $Fe_{\alpha-\varepsilon}$

There are very few data as for Fe transformation and 131-135 kbar has been long accepted as that value. However, the present value 114 ± 4 kbar quoted for the beginning of the transformation is 20 kbar lower than the above value. Although the value found by Stark and Jura[17] is somewhat larger than the present one, it should be worthy of note that $Fe_{\alpha-\varepsilon}$ is being found in the range 110 to 120 kbar. It is strongly hoped that much more data would be obtained for Fe.

(d) $Pb_{fcc-hcp}$

Table 4 shows transformation pressures for Pb obtained by several authors. A striking feature is the fact that, in spite of the significant differences between pressure generator types and also between the measuring principles, fairly good agreement is obtained for the $Pb_{fcc-hcp}$ in the pressure range 130-140 kbar. Here Drickamer's value is revised in the light of the data of Rice *et al.*,[20] the shock study on aluminum and silver powders, the P-V relationship for NaCl, and the compressibility data for MgO. Vereshchagin's pressure is also revised by taking the

Table 4. Summary of Pb transformation pressure data.

Author	Transformation pressure (kbar)		Pressure device
	increasing	decreasing	
NBS scale[6] (1968)	110 ~ 160		
Mao et al.[14] (1970)	130 ± 10	100 ± 10	diamond anvil
Vereshchagin et al.[8] (1970)	135 ~ 138		3-step apparatus
Drickamer[7] (1970)	128 ~ 132		Drickamer cell
Mii et al.[2] (1972)	137 ± 3	99 ± 2	Bridgman anvil
Yagi et al.[15] (1976)	142 ± 3	111 ± 2	cubic press

NBS Symposium scale of near 100 kbar transformations such as Bi_{III-V} and Sn_{I-II} into account. However, the NBS scale value for lead itself, 160 kbar, now appears to be too high compared with those summarized in Table 4.

The fact that the transformation pressure for lead obtained here agrees well with those obtained with the use of other types of pressure apparatus suggests that stress differences with Bridgman anvils are not much larger than with other types of apparatus.

Apart from some light thrown on the nonuniformity of pressure in the cell, the present result also offers a basis for the precise pressure determination by means of the NaCl internal standard technique.

Our experiment yielded 38 kbar as the value for the hysteresis of the transformation, $Pb_{fcc-hcp}$. Mao *et al.*[14] observed the very similar value of 30 kbar.

Further work should be devoted to a study of the dependence of hysteresis on such kinetic aspects as the loading rate, ambient temperature, and internal stress distribution within the cell.

1. 5. 2. Error estimation

According to Decker, the error in his P-V relationship for NaCl, on which the scale of the present study is based, can be estimated to be 1.1% up to 50 kbar, 1.7 % up to 100 kbar, and 2.4% up to 200 kbar. This assumes that the error in this relationship comes only from the estimated errors of the factors in the computation.

In the present experiment, errors would be expected to be primarily systematic, arising from the deviations of the sample cell from its original position during the compression, which is relevant for the Debye-Scherrer method of diffraction, and also from the random errors arising in the course of repetitive reading of the diffraction lines. This composite error affects the compressibility estimate for NaCl and is estimated to amount to 2.4 kbar at 100 kbar. The standard deviation in the lattice constants calculated from several diffraction lines is ~2 kbar.

A further error would arise if there were some pressure difference between the calibrant (NaCl), and the sensing element (bismuth, tin, iron and lead). It has been generally accepted that Bridgman anvils produce a much less uniform pressure within the cell than do multi-anvil type devices. But in any pressure generator which uses a solid pressure-transmitting medium a stress amounting to at least the flow stress of the solid is left in the cell, provided the medium deforms plastically. Thus the extent to which hydrostatic conditions are satisfied within the cell depends on the flow stress of the medium, regardless of the type of pressure generator used. For a rotating-anvil apparatus Bridgman[21] reported the flow stresses for NaCl, Bi, Sn, Fe, Pb and B as being 1.8, 0.75, 0.41, 5.2, 0.3 and 4.6 kbar at 20 kbar; and 3.0, 1.6, 0.77, 10.6, 0.68 and 18.0 kbar at 50 kbar, respectively. In the present experiment a very tiny plug of NaCl, 0.4 mm in diameter, was used as the calibrant. Thus, as far as shear stress is concerned, one would not expect a significant nonuniformity in the distribution of the axial stress along the pressing direction. Also, since the present NaCl plugs are surrounded by a boron disk having a larger flow stress, the axial stress will undergo a steep change in the boron portion of the cell which will tend to reduce stress differences in the NaCl portion.

1. 6. Conclusion

The pressures for the transformation Bi_{III-V}, Sn_{I-II}, $Fe_{\alpha-\varepsilon}$ and $Pb_{fcc-hcp}$ were determined as 76±4, 97±4, 114±4 and 137±3 kbar, respectively, for the upstroke

from the observed lattice contraction and Decker's new scale for NaCl. It is a notable feature at the present time that revisions of transition pressures for metals tend to be towards lower values. The present experimental results illustrate this well.

Chapter Ⅱ Pressure Effects on Phase Diagram of Al-rich Al-Si Alloys[22,23]

2. 1. Introduction

On pure metals many studies of pressure-induced transformations as partially described at the previous chapter, and of pressure-temperature phase diagrams, have been well known.[24,25] As for a binary alloy system there have been some studies of a pressure dependency on liquidus, solidus, eutectic point and solid solubility in Au-Cu, Fe-Ni, Fe-Si, Fe-C systems and so on.[26]

Under ordinary pressure the Al-Si alloy, known as an important casting alloy, is a simple substitutional alloy forming no intermetallic compound, and has a eutectic at 11.3%Si and 577℃. The solubility limit of Si in Al is 1.59% at the eutectic temperature, and the solubility of Al in Si is almost null.[27] (Unless otherwise noted, all compositions are expressed as atomic percentages through the present paper.)

While no work on this alloy system under high pressure has been reported, a lot of studies on the physical and metallurgical properties of this alloy have been made at ordinary pressure such as those of the precipitation of Si from Al-rich Al-Si alloys through the electron microscopy and the electric resistance measurement by Rosenbaum and Turnbull,[28,29] Ozawa and Kimura[30] and Van Gurp,[31] and that of the solubility limit of Si in Al through the electric resistance method by Kovacs-Csetenyi, Vassel and Kovacs.[32]

The present chapter is concerned with the experimental study of the high pressure phase diagram on the Al-rich Al-Si alloy system in which to determine in detail the liquidus, solidus and solvus of Si in Al. Also to obtain the supersaturated alloy, the specimens were quenched under high pressure. And then the X-ray diffraction, the micrographical observation and the hardness test were made on the quenched alloys.

In the present experiments a cubic anvil press have been mainly used as the high pressure apparatus, and the electric resistance of specimen has been precisely measured by means of a 4-probe method.

2. 2. Experimental

2. 2. 1. High pressure apparatus

In Fig. 3 is shown the high pressure apparatus which is composed of a 15 mm cubic anvil press of WC and the steel guide blocks. The top and bottom anvils are fixed to the blocks [5] and [6], respectively. Each of [5] and [6] has the 45°-inclined guide surfaces. The side anvil [1], dividing the vertical uniaxial load into components by the wedge action due to the inclined surfaces of the block, is advanced by the same amount synchronizing with the motions of the top and bottom anvils to the center of the pressurized cubic region. Each of the sliding surfaces between

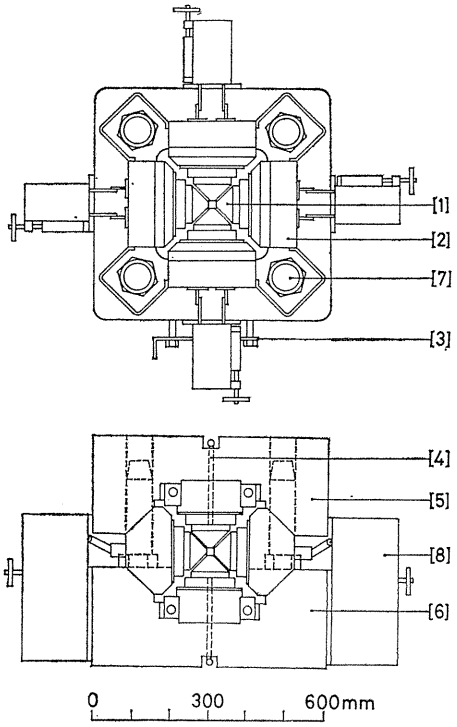

Fig. 3. Cubic anvil apparatus.
[1] Anvil,
[2] Anvil support,
[3] Current terminal for heating,
[4] Cooling water duct,
[5] Top guide block,
[6] Bottom guide block,
[7] Guide pin,
[8] Anvil puller.

the side anvils and the guide blocks is well lubricated by both of MoS_2 and Teflon sheet. The motions of the top and bottom guide blocks are precisely aligned by means of four robust guide pins each 65 mm in diameter. This high pressure apparatus is driven by a 1200 ton hydraulic press equipped with a constant loading controller.

The current for heating sample is supplied from a 3 kW source whose power is controlled by means of the Hall element and the thyristor. This current flows from the heating current terminals [3], which contact to the top and bottom anvils, respectively. And then it flows in the cylindrical carbon heater within the pressure cell. To prevent the overheating of the anvils, cooling water circulates in the top and bottom anvil blocks through the ducts [4].

A girdle type high pressure device[33] have been partially used in the experiments at pressure of 28 kbar.

2. 2. 2. Pressure cell and samples

In Fig. 4 is shown the assembly of the pressure cell for the cubic anvil press. The cell whose edge was 20 mm long each was formed from the pyrophyllite baked at 500℃ for 1 h. The electric current for heating the sample flows through copper rings to the carbon heater. Inside the cylindrical carbon heater a sleeve and disks of boron nitride (BN), the alloy sample and a Pt-Pt13%Rh thermocouple of 0. 3 mm o. d. were inserted. A pure aluminum wire 0. 3 mm o. d. was used as the lead-wire for measuring the electrical resistance, and each of the current and potential difference lead-wires was connected to one of the four anvils. The BN and the carbon was preheated in vacuum at 1000℃ for 1 h for evacuating gases in advance.

Both of the aluminum lead-wire and the thermocouple were insulated from the carbon heater by means of the thin BN tubes 2 mm o. d.. The thermocouple was taken out through the gap between the anvils.

The another cell assembly for the girdle type high pressure device is shown in Fig. 5. Inside the cylindrical pyrophyllite of 12.4 mm o. d. and 7 mm i. d., a carbon heater, pressure transmitting medium made of BN, a thermocouple and the specimen. This cell assembly and high pressure device were only used for a part of the experiments at the pressure of 28 kbar, so that the following description of the experimental procedure will be confined to the cubic anvil press.

Sample alloys were prepared by following ways. The mixture of zone-refined 99.999% Al and 99.999% Si in the desired composition was melted in an alumina crucible. In this process the mixture of NaF and NaCl was floated on the molten alloy as flux to prevent the oxidation of alloy. And then molten alloy was sucked in 3 mm i. d. Pyrex tube, and was solidified in situ. Compositions of the sample alloys thus obtained were determined to be Al-1.1, 2.5, 3.7, 7.0, 11.4 and 14.9% Si by the wet analysis. To make the samples for measuring electric resistance, these cast alloys and pure Al were rolled into thin pieces 0.01 mm thick, 6 mm long and 0.5 mm wide, and then annealed in vacuum at 400°C for 3 h to release any residual

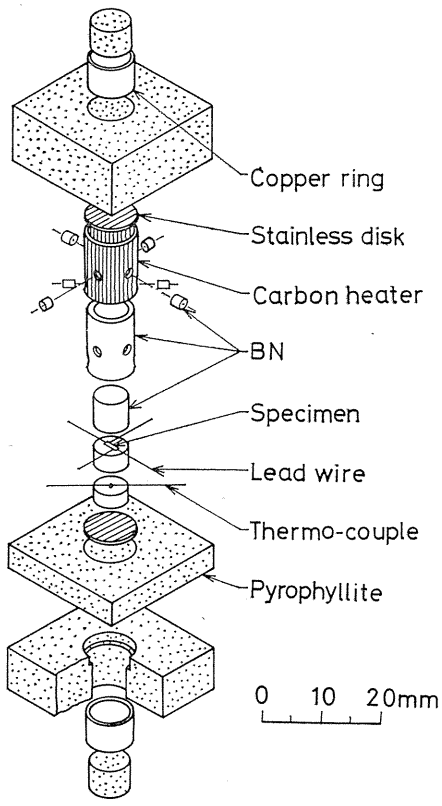

Fig. 4. Pressure cell assembly for measurements of electrical resistance used on the cubic anvil apparatus.

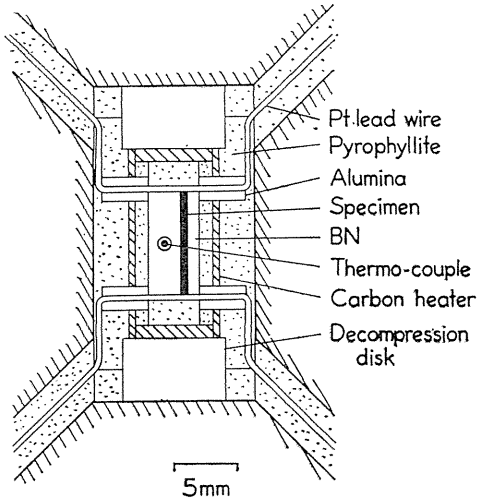

Fig. 5. Pressure cell assembly used on the girdle type apparatus.

stress or strain. And 1.5 mm d. wire-drawn sample alloys were also used as the samples for X-ray measurement, microscopic observation and hardness testing. The grain size of the sample alloy and pure Al was about 0.02 mm.

2. 2. 3. Experimental procedures

Through the experiments on the cubic anvil press the load was increased at a fixed rate 8 ton/min until the fixed load value 300 or 800 ton was attained. The press load of 300 and 800 ton were calibrated to 28 and 54 kbar, respectively, at the sample site by using the fixed points such as $Bi_{I\text{-}II}$ (25.4 kbar), $Tl_{II\text{-}III}$ (36.7 kbar) and $Ba_{I\text{-}II}$ (55 kbar).

The sample was heated at a rate of 2℃/min. In addition to record the electric resistance of the sample continuously, precise resistance measurements were performed by a digital micro-voltmeter every 50℃ steps keeping constant temperature for 30 min to 2 h. This time duration was required to solution of Si in Al. In the present 4-probe method, by flowing a calibrated constant current 100.000 mA the potential difference between the both ends of the sample could be read with five digits. Also to avoid the errors such as due to the thermal emf and the contact potential difference, the resistance measurement was made several times by alternating the current direction.

To confirm the solution of Si in Al the quenching of the sample from high temperature and high pressure to the ordinary temperature and pressure was performed. Sample alloys Al-7.0% Si were solution-treated at 54 kbar by three ways such as 420℃ for 2 h (denoting 2HR420), 420℃ for 10 h (10HR420) and 600℃ for 2 h (2HR600). These samples were quenched to room temperature by shutting off the heating current with a cooling rate of about 140℃/sec. The quenched samples were examined by the X-ray diffracion measurement, the microscopic observation and the Vickers-hardness testing.

And to determine the solubility limit of Si in Al also by means of the quenching method, the alloys having several Si-components were quenched from various temperatures of the solution-treatments under high pressures.

2. 3. Results and discussions

2. 3. 1. Temperature dependence of electric resistance

In Fig. 6 is shown the electric resistance vs. temperature relationship obtained by the pure aluminum. R_t/R_0 in the ordinate means the ratio of the resistance value at T℃ to the value at room temperature. The curve was taken during the first time heating after the pressurization to 54 kbar.

In the pure aluminum the resistance increases linearly with temperature up to 200℃, and after that its temperature derivative decreases slightly and the resistance maximum is attained at about 420℃, but the resistance increases again linearly from 500℃ to the melting point. To examine the apparent resistance anomaly in the range from 200℃ to 500℃, measurements of electric resistance were continued between the room temperature and 600℃ repeating alternate heating and cooling. As shown in Fig. 7, a linear relationship was obtained at the second time heating. Though the causes of the resistance anomaly shown in the first run can not be elucidated in the present experiments, it should be considered that the sample is much or less affected by the complex shear stresses and strains and some lattice defects due to the deformation during the pressurization. This anomaly, therefore,

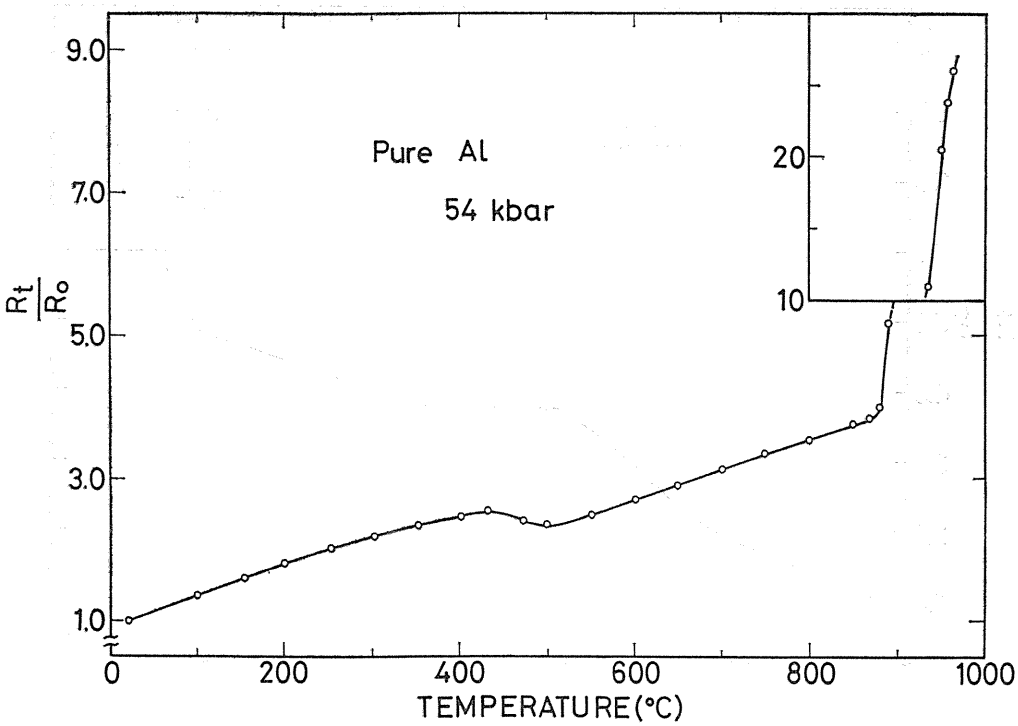

Fig. 6. Electric resistance vs. temperature relationship of pure Al at 54 kbar.

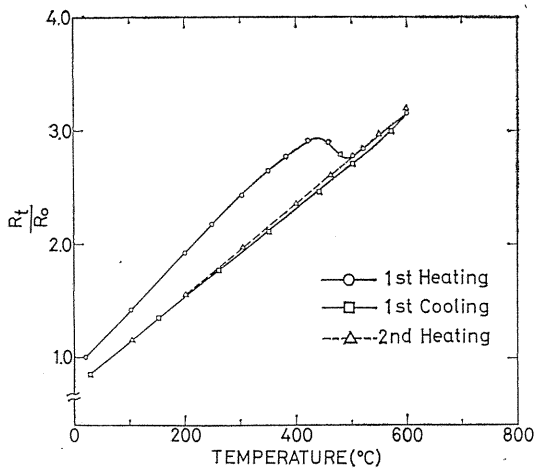

Fig. 7. Electric resistance change by alternate heating and cooling cycles on pure Al at 54 kbar.

should be taken place by the recovery of their shear stresses or defects.

The electric resistance vs. temperature relationship of Al-7.0% Si alloy was shown in Fig. 8. In this case the temperature derivative of the resistance was increased from 200℃ by the solution of Si in Al. The resistance increment due to

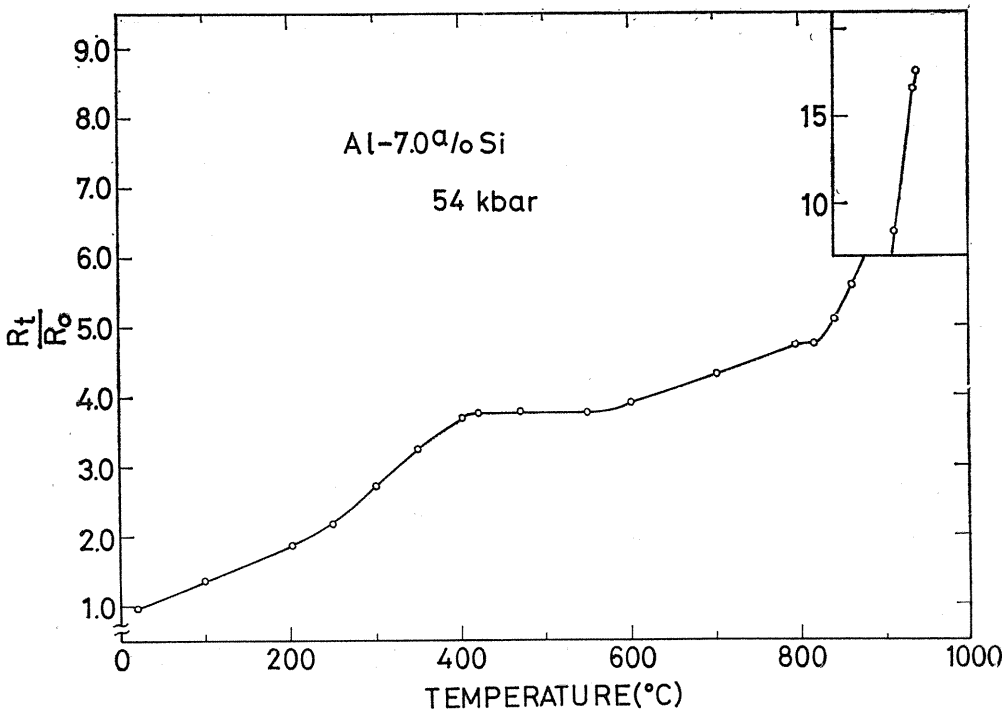

Fig. 8. Electric resistance vs. temperature relationship of Al-7.0% Si alloy at 54 kbar.

the solution of Si, however, was superposed on the recovery of the resistance over the range from 200℃ to 500℃. Thus it was hard from Fig. 8 to identify the solid-solubility of Si. Moreover in this experiment Si could not be precipitated from the solution even by annealing at 200℃ for 10 h under 54 kbar. It was, therefore, impossible to detect the resistance increment due to the solution of Si by the second time heating process as shown in Fig. 7.

Both of the liquidus and the solidus, on the other hand, could be readily assigned from Fig. 8 to 930℃ and 820℃, respectively. Thus obtained the liquidus, solidus and eutectic temperatures are summarized on Table 5 for the pressure of 28 kbar and on Table 6 for 54 kbar.

Table 5. Liquidus, solidus and eutectic temperature of Al-Si alloy at pressure of 28 kbar.

Si %	Liquidus	Solidus	Eutectic
0	840 ℃		
1.1	835 ℃	785 ℃	
1.2	820 ℃	730 ℃	
3.7	820 ℃	710 ℃	
7.0	790 ℃		660 ℃
11.4	740 ℃		660 ℃
14.9	710 ℃		660 ℃

Table 6. Liquidus and solidus temperature of Al-Si alloy at pressure of 54 kbar.

Si %	Liquidus	Solidus
0	970 ℃	
3.7	940 ℃	910 ℃
7.0	930 ℃	820 ℃
11.4	900 ℃	790 ℃
14.9	890 ℃	700 ℃

These temperatures are measured by the Pt-Pt-13% Rh thermocouple under high pressure. Though emf of thermocouple is affected by pressure in general, in the present experiment the pressure effect of emf is not taken into account, since it is too difficult to correct exactly. It is considered that these temperatures give the lower values by about 5% at 54 kbar.[34,35]

2. 3. 2. Solubility limit of Si in Al

Just as mentioned above it is very hard to identify directly the solubility limit of Si in Al from the electric resistance vs. temperature measurements. Here by taking the difference in the shape among the sample into account, the resistance vs. temperature relationship has been first transferred to the resistivity vs. temperature relationship. Then from the resistivity difference between the pure Al and the alloy at an identical temperature the resistivity increment $\Delta\rho_{Si}$ accompanied with solution of Si in Al has been obtained.

The electric resistance R_{Al} of the pure Al and $R_{Al\text{-}Si}$ of the alloy would be expressed as follows;

$$R_{Al}=k_s(1+\alpha T)\rho_{Al}, \tag{2}$$

$$R_{Al-Si}=k'_s(1+\alpha T)\rho_{Al}+k'_s\Delta\rho_{Si}, \tag{3}$$

where k_s and k'_s are coefficients depending on the sample shape, T the temperature and ρ_{Al} and α the resistivity of the pure Al annealed under high pressure and its temperature coefficient, respectively. From eqs. (2) and (3), the resistivity increment accompanied with solution of Si in Al is expressed as

$$\Delta\rho_{Si}=R_{Al-Si}/k'_s-R_{Al}/k_s \tag{4}$$

In the present study k_s and α have been determined from eq. (2) by the present measurements of R_{Al} at 20℃ under 54 kbar, along with the value of $\rho_{Al}=2.25$ $\mu\Omega$cm at 20℃ under 54 kbar. This value of ρ_{Al} at 54 kbar is reduced from resistivity 2.75 $\mu\Omega$cm at 0 kbar using Bridgman's measurement[36] of electric resistance vs. pressure relationship. Also from eq (3) k'_s and $\Delta\rho_{Si}^{max}$, the resistivity increment at the completely dissolved state of Si into Al, have been determined using the ρ_{Al} and α just obtained. Meanwhile with the values of R_{Al} and $R_{Al\text{-}Si}$ measured during the first time heating along with the pertaining values of k_s and k'_s, eq. (4) gives the numerical values of the resistivity increment $\Delta\rho_{Si}$ due to the solution of Si in Al.

Figure 9 shows the $\Delta\rho_{Si}$ vs. temperature relationship thus obtained. The figure reveals that the solution of Si in Al begins at about 200℃ and then the $\Delta\rho_{Si}$ value

is increased along the solubility limit up to its saturated value $\Delta\rho_{Si}^{max}$. The fact that there is a slight inconsistency in the solubility limits of the samples tested should be attributed to that the thermal equilibrium of the sample has not been attained completely due to the extremely low mobility of Si in the alloy under high pressure.

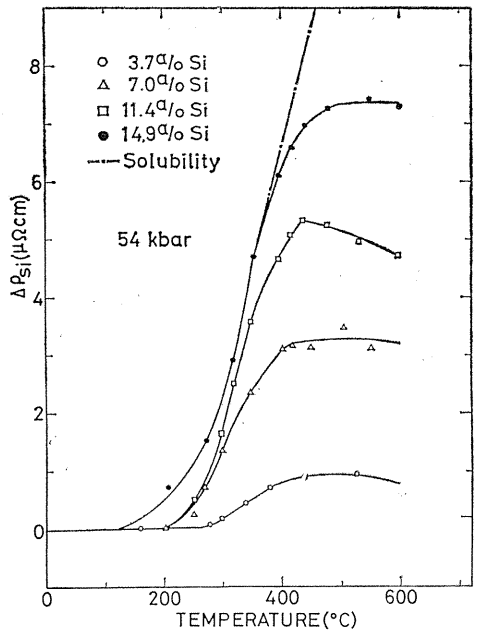

Fig. 9. Resistivity increment, $\Delta\rho_{Si}$, due to solution of Si in Al as a function of the temperature.

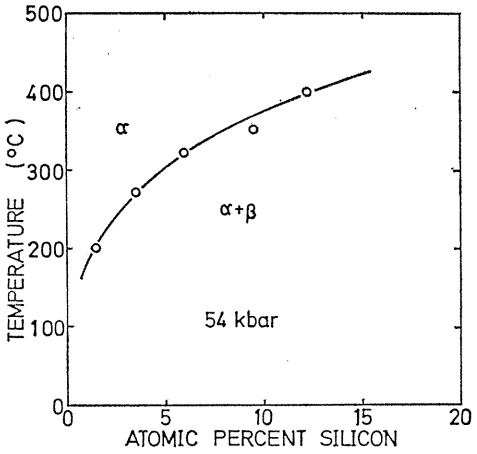

Fig. 10. Solubility limit of Si in Al under pressure of 54 kbar.

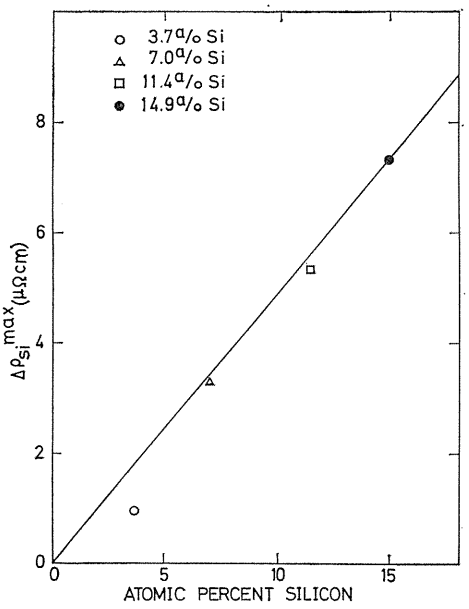

Fig. 11. Maximum of $\Delta\rho_{Si}$ in Fig. 9, $\Delta\rho_{Si}^{max}$, as a function of Si-concentration.

Since the most reliable measurement of $\Delta\rho_{Si}$ in Fig. 9, therefore, would be on the sample Al-14.9%Si, the solvus line was determined from the measurements on Al-14.9%Si as shown in Fig. 10.

In Fig.11 is shown the $\Delta\rho_{Si}^{max}$ vs. Si-content relationship. The scattering of these measured points is not so large that the before-mentioned procedure for determining the solubility limit of Si would be reasonable. From the slope of this relationship 0.5 $\mu\Omega$cm/%Si is obtained as the resistivity increment due to the solution of Si in Al at 54 kbar. In comparison with the value 0.7 $\mu\Omega$cm/%Si by Kovacs-Csetenyi *et al.*[32] at 0 kbar, the resistivity increment should be decreased at high pressure. Along with the fact that the resistivity of metals is decreased with pressure in general, the present result should be reasonable.

2. 3. 3. Quenching of samples

To confirm the solid-solution of Al(Si), quenching from high temperature under high pressure was performed on the Al-7.0%Si alloy on which the existence of the precipitated Si has been examined by the X-ray diffraction. As shown in Fig. 12, the results were such that while the faint diffraction lines of Si remained in 2HR420

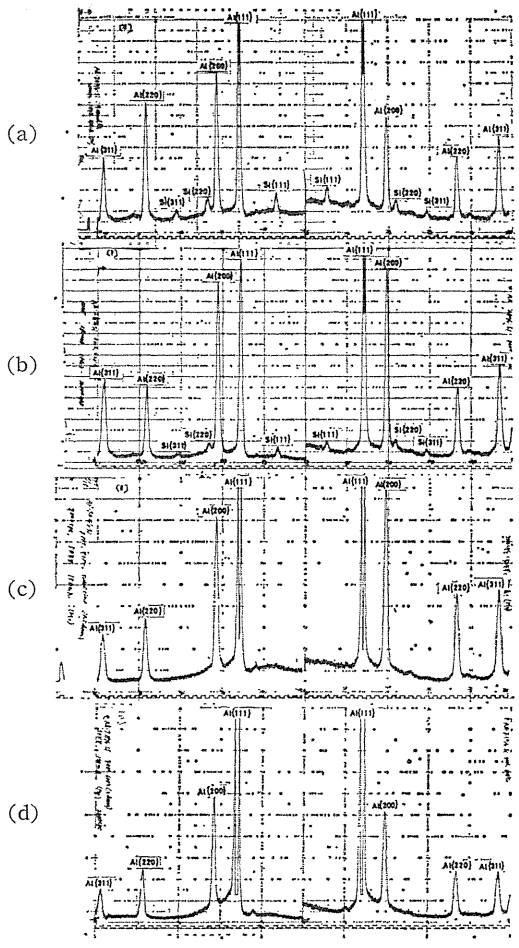

Fig. 12. X-ray diffraction profile of Al-7.0%Si alloy quenched from high temperature and high pressure.
(a) Starting material,
(b) 2HR420,
(c) 10HR420,
(d) 2HR600.

showing an incomplete solution-treatment, they disappeared completely for the specimens 10HR420 and 2HR600. This shows that a longer time should be needed to make solution of Si in Al under high pressure, but the solid-solution of Al(Si) could be quenched to the ordinary temperature and pressure. Since the precipitated Si in the quenched alloy sample except 2HR420 was not also detected by the micrographical examination, the above results were supported.

Vickers-hardness testing was also performed on the quenched samples, giving H_V = 61, 82 and 83 for samples 2HR420, 10HR420 and 2HR600, respectively. Comparing to the original hardness H_V=41 of the annealed alloy, the hardness of the solution-treated alloy was almost doubled.

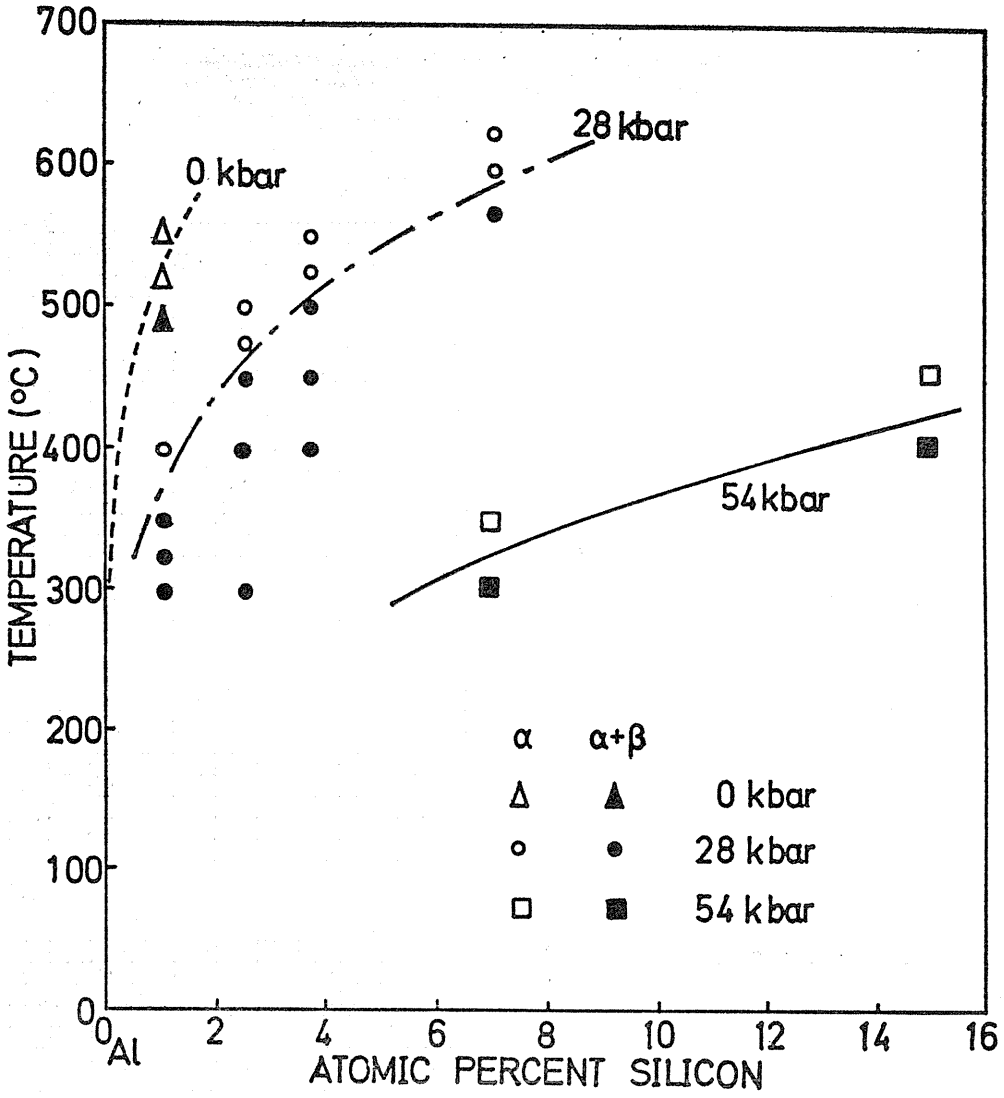

Fig. 13. Solubility limits of Si in Al under pressure of 28 and 54 kbar by means of the quenching method.

Next the solubility limits of Si in Al were investigated by means of the quenching method under pressures of 0, 28 and 54 kbar. As shown in Fig.13 the results of quenching were fairly agreed with Hansen's phase diagram at 0 kbar and the results of the electrical measurements at 54 kbar described in the previous section. The solubility limits of Si in Al at 28 kbar, therefore, were determined by the quenching experiments. These obtained values were summarized in Table 7. The solubility limit of Si in Al was markedly extended beyond 15% at 54 kbar in comparison with 1.59% at 0 kbar.

Table 7. Solvus temperature of Si in Al under high pressure.

Si %	0 kbar	28 kbar	54 kbar
1.1	530 ℃	370 ℃	
2.2		490 ℃	
3.7		520 ℃	280 ℃
7.0		580 ℃	320 ℃
11.4			380 ℃
14.9			420 ℃

2. 3. 4. High pressure phase diagram

In Fig.14 the Al-side phase diagram of Al-Si system obtained in the present

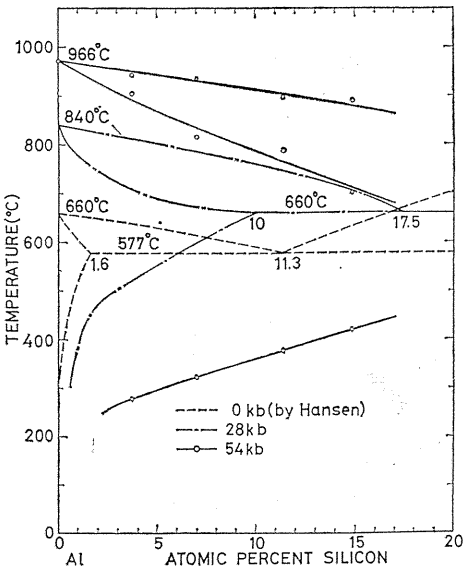

Fig. 14. Al-side phase diagram of Al-Si alloy at high pressure.

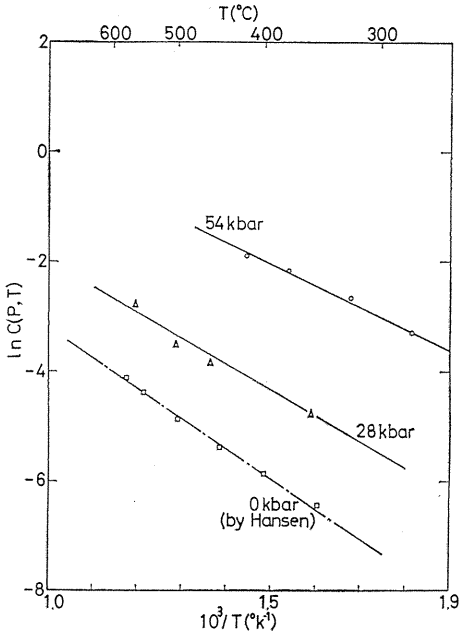

Fig. 15. Solute Si-concentration in Al as a function of the reciprocal temperature.

study is shown in comparison with those at 0 kbar. The melting points of the pure Al increase to 840℃ at 28 kbar and 970℃ at 54 kbar from 660℃ at 0 kbar giving the mean pressure derivatives 6.4℃/kbar (0 to 28 kbar), 5.7℃/kbar (0 to 54 kbar) and 5.0℃/kbar (28 to 54 kbar). The pressure dependence of the melting point is diminished with increasing pressure.

In Fig.15 are shown solute Si concentration vs. reciprocal temperature relationships obtained from the data of solubility limits on Table 7. According to Fig. 15 the logarithm of the solute Si concentration is a linear function of the reciprocal temperature. This means that the solute concentration C can be written as

$$C=C_0\exp\ (-\Delta H/kT), \tag{5}$$

where ΔH is the activation enthalpy for solution. From Fig. 15 we find 0.39 eV at 28 kbar and 0.32 eV at 54 kbar. Compared with 0.46 eV at 0 kbar, it is found that the activation enthalpy for solution of Si in Al is decreased with increasing pressure.

The activation enthalpy ΔH should be written as $\Delta H=P\Delta V+\Delta E$, where P is pressure and ΔV and ΔE are the activation volume and energy for solution, respectively. Since the lattice of Al is contracted by the solution of Si,[37] ΔV should be nagative. Then the present result for the pressure dependency of the activation enthalpy seems to be reasonable.

2. 4. Conclusion

In making use of a girdle type anvil and a 15 mm cubic anvil apparatus, a phase diagram of Al-rich Al-Si alloy was determined under 28 and 54 kbar. Samples employed were a pure Al and Al-Si alloys containing Si ranging from 1.1 to 14.9%. The liquidus, the solidus and the solvus of Si in these alloys were determined by means of the 4-probe measurement of the electric resistance and the quenching method.

Results obtained follow;

(1) The melting point of pure Al increases to 840℃ at 28 kbar or 970℃ at 54 kbar from 660℃ at 0 kbar with the mean pressure derivative of 5.7 ℃/kbar.

(2) It was shown that the solid solubility of Si in Al was extended to 15% at 54 kbar from 1.6% at 0 kbar by the electric resistance measurements. The resistivity increment due to the solution of Si in Al was 0.5 $\mu\Omega$cm/%Si under the pressure of 54 kbar. The activation enthalpy for solution of Si in Al, which was obtained from the data of solubility limits, was 0.39 eV at 28 kbar or 0.32 eV at 54 kbar, and it was decreased with increasing pressure.

(3) Completely solution-treated Al-7.0%Si samples have been quenched from high temperature at high pressure. X-ray diffraction and the microscopic examination made on these samples show that Si has been completely dissolved into the Al matrix. Vickers-hardness testing was also made on these alloys showing that the hardness of the quenched alloy has been doubled compared to that of the annealed alloy.

Chapter Ⅲ Pressure Effects on Atomic Vacancies of Platinum[38]

3. 1. Introduction

Atomic vacancies have a number of important effects on crystal properties.

They are involved in the processes of diffusion, they contribute to electrical and thermal resistivity, and they play a role in void growth during plastic deformation. Through their interaction with dislocations they have an effect on the mechanical properties of metals. The importance of atomic vacancies rests on their critical presence in many metallurgical and solid state phenomena. Thus, the questions of their concentration as a function of temperature and pressure and its relation to thermodynamic factors is of great interest.

For the study of atomic vacancy concentration and its effect to the properties of crystalline metals, previous authors have used the quenching method. If the specimen is quenched so fast as to freeze those defects and subsequently held at a sufficiently low temperature, it should involve some excess vacancies and will exhibit a larger electrical resistivity than the annealed one. When the concentration of vacancies in a solid is not so high, the electrical resistivity increment should be proportional to that concentration. Thus, by measuring the resistivities of the specimen before and after quenching, one can deduce the concentration of vacancies presented in a specimen at the quenching temperature.

The quenching method on metals was first introduced by Koehler *et al.*[39~41] in 1950's at atmospheric pressure, and has been used so far to study the concentration and the diffusion rate of thermally-produced vacancies in various metals such as gold, platinum, aluminum, silver and so on. However, because of many technical difficulties under high pressure, only a few experiments under gas pressures up to about 6 kbar have been reported by Huebener,[42] Emrick *et al.*[43,44] and Charles *et al.*[45]. Especially under very high pressure exceeding 30 kbar where almost pressure media must be solidified no result has been reported in spite of its great inherent interest for solid state physics.

The present study is concerned with the quenching experiments for platinum wire under very high pressures using a solid as a pressure transmitting and cooling medium. In the present chapter are first described the geometry and quenching performance of the high pressure cell adopted which permits a four-probe electrical resistance measurement between the Bridgman-type anvils. Results on the energy and volume of the vacancy formation in platinum thus obtained are also presented.

3. 2. Experimental

3. 2. 1. Experimental apparatus and high pressure cell

The Bridgman-type anvils made of tungsten carbide with working flat face of 10 mm d. which were triply bound by high tensile steel rings were used for the high pressure quenching experiments.[46] One of the technical difficulties in the experiment was to measure an electrical resistivity of a specimen with necessary precision. This was overcome by making use of a four-probe method in a distortion- and contamination-free environment.

Figure 16 shows the assembly of the high pressure cell. It consists of a specimen of 99.999% pure Pt wire of 0.05 mm d., potential leads of 0.05 mm d. Pt wire, current leads of Pt foil, pressure transmitting and cooling medium of BN, pyrophyllite gaskets, and stainless steel rings. The 0.3 mm thick stainless steel rings flattened and work-hardened to $H_v=380$ were used as a pressure container. These rings also serve as two electrical potential leads of the four-probe method. For the electrical insulation between rings and upper and lower anvils and for the pressure sealing, disks and rings of baked pyrophyllite were employed. Previous

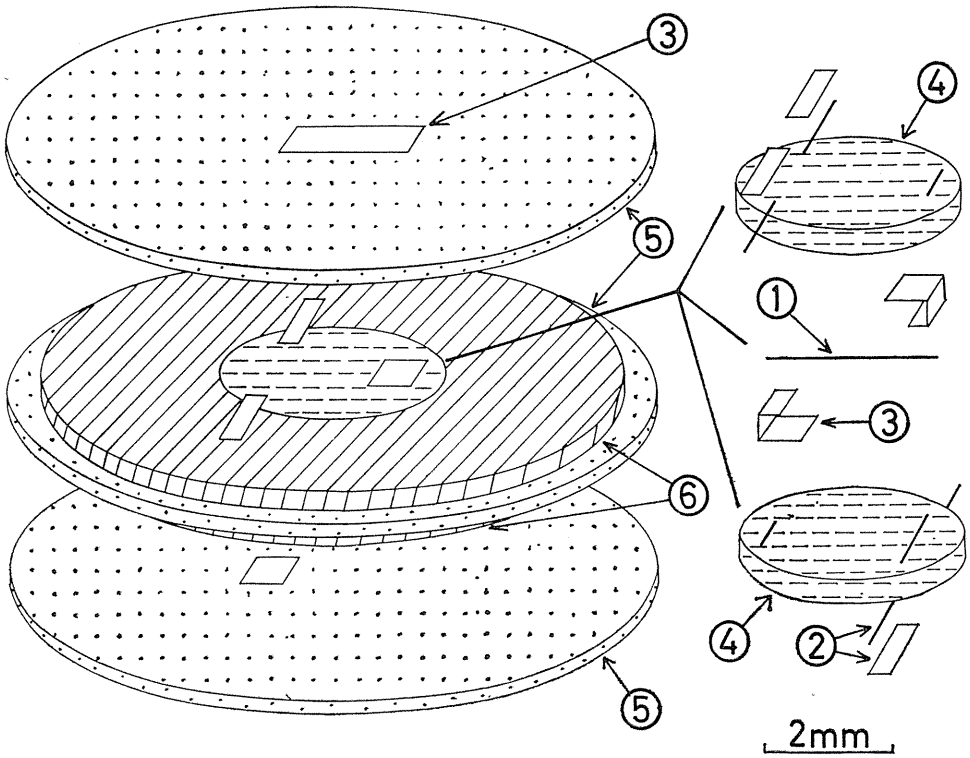

Fig. 16. Pressure cell assembly for vacancy study.
(1) platinum specimen, (2) platinum potential leads,
(3) platinum current leads, (4) boron nitride disks,
(5) pyrophyllite gaskets, (6) stainless steel rings.

workers have tried a four-probe method having leads through the sides of the pyrophyllite gaskets directly into the sample in the Bridgman type anvils.[47~49] In the present experiment, however, the stainless steel rings themselves formed the potential leads of the four-probe method, and have been satisfactorily used for measuring the accurate electrical resistivity of the specimen without pinching off or making any short circuit even in such a high pressure as 120 kbar.

One of the key points for the present high pressure quenching experiment was to select an appropriate material for the pressure transmitting and cooling medium. Aptitudes to be fulfilled for the material should be good electrical insulation, heat conduction to secure the rapid cooling and the temperature uniformity along the wire specimen, contamination- and reaction- resistance to the specimen under high pressure and tempereture, and relaxation for the complex shear stress by the applied force to realize a quasi-hydrostatic pressure. Since BN is known as a superior crucible material at atmospheric and higher pressure, the hot pressed BN (Denki-kagaku Type-HC) was employed as the medium in this experiment.

The specimen wire was inserted between two BN disks 3.5 mm in dia. and 0.4 mm thick. To avoid the distortion of the specimen during the loading a groove and a hole were carved on each of the BN disks, and the specimen wire and leads were tightly buried in them. To prevent the BN disks from fracturing and bulging out

of the cell under applied pressure, the total thickness of two BN disks were made smaller than those of the pyrophyllite and two stainless steel rings by 0.02 mm. By experience it should be stated that these parts must be formed very precisely and set up into the cell with a special care. When the clearance between the BN disks and pyrophyllite disks were too wide, the pressure-sealing pyrophyllite ring flew out of the contact surface of the disks and cut down the specimen wire and leads, and when that was too narrow, the stainless steel rings were broken.

3. 2. 2. Measurements of electrical resistance

Electrical resistances of the specimen before and after quenching were measured at room temperature by means of a null-detector and a four-dial double bridge whose potential leads were connected to the above-mentioned two stainless steel rings of the cell. Current of 0.05 A was applied to the specimen through anvils. To cancel an effect of thermo-electric power, polarity of the measuring current was alternately changed several times. The smallest detectible change in the specimen resistance of 0.1 Ω was 10^{-7} Ω which was about 0.01% of the maximum quenched in resistance increment. In order to eliminate the variation in the thermal portion of the specimen resistance arising from the temperature fluctuation, the resistance of the specimen was usually compared to that of the dummy which was held under the same condition as the specimen. In the present experiment, however, it was hard to use the dummy of exactly identical configuration and resistance to the specimen because of the smallness of the high pressure cell along with the difficulty of assembly. To estimate the specimen temperature a thermistor thermometer which was calibrated from 0 to 100℃ was fitted to the anvil shoulder which was closely adjacent to the cell.

The specimen was heated directly by 10 to 12 A of dc applied from a stabilized dc power supply through the upper and lower anvils. Specimen temperature during the heating was measured by the ratio of the specimen resistivity at high temperature during the heating was measured by the ratio of the specimen resistivity at high temperature to the one at room temperature refering to the temperature coefficient of resistivity of Pt[50] without pressure compensation.

The pressure within the cell was calibrated by using three pressure fixed points of Bi_{I-II}, Bi_{III-V} and $Fe_{\alpha-\varepsilon}$.[1,6] By putting the calibrant metal at different points across the diameter of the BN disks, it was also confirmed that the pressure gradient in the cell was negligibly small. The resistivity variation of the Pt specimen with pressure agrees within ±1% with the Bridgman's data[51] up to 100 kbar.

3. 2. 3. Quenching

Cell was pressurized very gradually to a desired value. The Pt wire in the cell was annealed at 1000℃ for 10 min to eliminate the internal stresses along with the presumable defects coming from the loading. The quenching process itself was rather simple. After heating the wire specimen up to the desired quenching temperature, 1000 to 1350℃, we kept that temperature for 3 min, and then turned off the current. By the thermistor thermometer it was found that the specimen temperature immediately after quenching was about 50℃. By leaving it as it stands, however, the specimen was cooled to such an extent that the difference from room temperature was almost disappeared. A very slight difference remained was corrected by using the temperature coefficient of the electrical resistivity near room temperature. The variation of the specimen resistivity was less than 0.01%

for repetitive quenching and annealing cycles. This is only 2 to 3 % of the quenched-in resistivity increment. Annealing for the purpose of extinguishing the resistivity increment due to the quenched-in excess vacancies was such that the specimen heated to 800℃ for 5 min was cooled very slowly to room temperature.

Measurements of the quenching rate were made by the same scheme which Bauerle and Koehler[41] used, i. e., the specimen potential leads were connected to the vertical deflection input of an oscilloscope, and in place of turning off the heating current entirely at the quenching, some portion about 0.1 A was left as the current for measuring the electric resistance of the specimen. A graphical plot of the specimen temperature versus time was then obtained, since the resistance variation during the quenching was translated to the temperature variation.

3. 3. Results and Discussions

3. 3. 1. Cooling rate of quenching

In Fig. 17 are shown a typical cooling curve when the specimen was quenched from 1050℃ under 30 kbar. It is clear that these cooling curves differ significantly from those of water quenching. In water quenching three stages would be seen; stage I where wire is shielded by water vapor layer, stage II where the vapor transfers to bulk liquid from wire and stage III where wire is convectively cooled by bulk liquid.[52] Contrary, the quenching in solid BN shows maximun cooling rate immediately at the quenching temperature and its temperature decreases almost exponentially toward room temperature. Thus to obtain a higher cooling rate it should be much more advantageous to cool sample within BN than in water.

The average cooling rates between T_q, the quenching temperature, and $T_q/2$

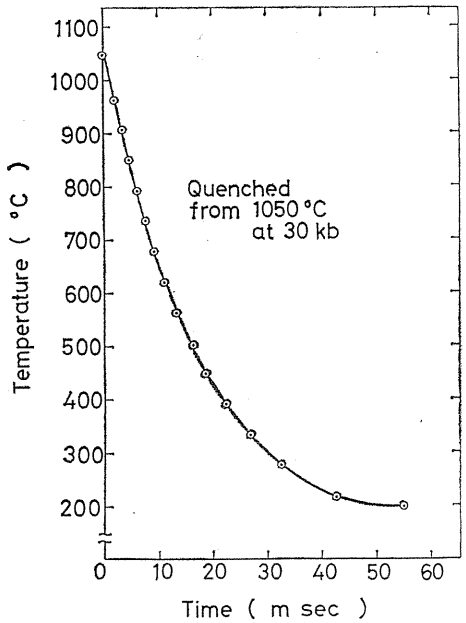

Fig. 17. Typical cooling curves of quenching in solid under high pressure.

were about 3.5×10^4℃/sec. This value is almost comparable to those of Pt quenched into water by Jackson.[52]

3. 3. 2. Quenched-in resistivity increment

It is well known that the equilibrium vacancy concentration C at temperature T and pressure P, can be described by

$$C(P,\ T)=\exp[\Delta S_f/k]\exp[-(\Delta E_f+P\Delta V_f)/kT], \tag{6}$$

where ΔE_f, ΔV_f and ΔS_f are the change of the internal energy, the volume and the vibrational entropy of the crystal required to form a vacancy, respectively. k is Boltzmann's constant. When it is reasonable to assume that the resistivity increment by quenching is in proportion to the vacancy concentration and the whole vacancies are retained during quenching, eq.(6) will be rewritten to the following expression,

$$\Delta R/R=A\exp[-(\Delta E_f+P\Delta V_f)/kT_q], \tag{7}$$

where $\Delta R/R$ is the quenched-in resistivity increment, T_q is the quenching temperature and A is the entropy factor.

To confirm the adaptability of eq.(7) to the observed values of quenched-in resistivity increment, one may plot the data as $\ln(\Delta R/R)$ vs. $1/T_q$. As shown in Fig. 18, under 0 kbar the points just fell on a straight line for quenching temperature from 1000 to 1350℃. Thus values of ΔE_f and A could be obtained from the slope and intercept of this line with the ordinate respectively. Under 30 kbar, however, a few points for higher temperature range came off a straight line drawing slightly

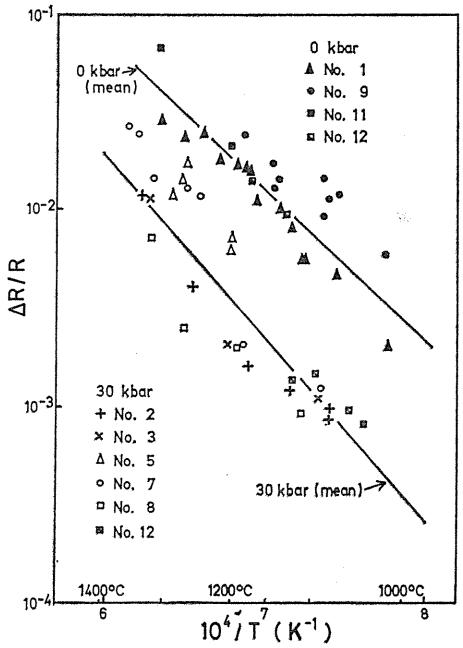

Fig. 18. Semilogarithmic plot of quenched-in resistivity vs. reciprocal of the absolute quenching temperature.

upward concave curve. Possible causes to this disagreement would be as follows; the temperature coefficient of the resistivity of Pt was not corrected for the pressure, and some other defects besides the thermal equilibrium vacancy such as those due to thermal strain and chemical contamination might be induced to the specimen. Disregarding the disagreement, one can draw a straight line for each cell by a least squares method. In Fig. 18 are shown lines thus drawn for the experiments at 0 or 30 kbar from which one can obtain values of $\Delta H_f = \Delta E_f + P\Delta V_f$ and A. While these values varied slightly among different cells, the averages were;

$$\Delta E_f = 1.52 \pm 0.06 \text{ eV}$$
$$A = 3.47 \pm 0.20 \qquad \text{at 0 kbar,}$$

and

$$\Delta H_f = 1.84 \pm 0.07 \text{ eV}$$
$$A = 3.83 \pm 0.26 \qquad \text{at 30 kbar.}$$

Very recently we have been performed such experiments under higher pressure of 60 kbar by making use of cubic anvil press.[53] On Table 8 these values are compared with those of the other experiments quenched into water and with calculated values.

Table 8. Vacancy formation energy ΔE_f on Pt.

Author		Pressure (kbar)	ΔE_f (eV)	Quenching medium
Bradshaw *et al.*[88]	(1956)	0	1.4 ±0.1	Water
Ascoli *et al.*[89]	(1958)	0	1.23	Water
Bacchella *et al.*[90]	(1959)	0	1.20±0.04	Water
Jackson.[52]	(1964)	0	1.51±0.04	Water
Mii *et al.*[91]	(1970)	0	1.05	Water
Senoo *et al.*[38]	(1973)	0	1.52±0.07	Solid BN
〃		30	1.84±0.07	Solid BN
Senoo *et al.*[53]	(1976)	60	2.18±0.04	Solid BN
Mii *et al.*[92]	(1976)	0	1.73	Calculation
〃		30	1.87	Calculation

According to the eq. (7) the change of the equilibrium vacancy concentration with pressure is given by

$$\partial \ln C/\partial P = -\Delta V_f/kT, \tag{8}$$

which yields Huebener's relation[42]

$$C(P, T) = C(P_0, T)\exp[-\Delta V_f(P-P_0)/kT]. \tag{9}$$

Substituting the experimental data to this equation, the vacancy formation volume ΔV_f can be obtained. The result at 1100℃ was $\Delta V_f = (1.18 \pm 0.14) \times 10^{-23}\text{cm}^3/\text{atom}$ (0.77 ± 0.09 atomic volume). This value seems reasonable compared to the other quenching experiments under gas pressure. These features are summarized on Table 9.

Table 9. Vacancy formation volume ΔV_f by high pressure quenching method for various metals.

Author	Material	Pressure (kbar)	Quenching medium	ΔV_f (cm³/atom)	Fraction of atomic volume
Huebener[42] (1964)	Au	11	rare gas		0.53 at 680 ℃
Emrick *et al.*[43] (1969)	Au	6	Ar gas	1.13×10^{-23}	0.65 at 640 ℃
〃	Al	6	Ar gas	1.06×10^{-23}	0.62 at 420 ℃
Emrick[44] (1972)	Pt	6	Ar gas	1.06×10^{-23}	0.70 at 1100 ℃
Senoo *et al.*[38] (1973)	Pt	30	solid BN	1.18×10^{-23}	0.77 at 1100 ℃
Charles *et al.*[45] (1975)	Pt	8	He gas		0.69 at 800 ℃
Senoo *et al.*[53] (1976)	Pt	60	solid BN	1.12×10^{-23}	0.74 at 1100 ℃

3. 3. 3. Boron nitride as pressure transmitting medium

As the results in the vacancy study are sensitively affected by contamination of the specimen from its environment, it is feared that even BN generally known as a superior crucible material might be a contamination source in the present experiment. Though we could not directly examine the extent of the contamination of the quenched specimen, at temperatures lower than 1400℃ the specimen resistance was substantially stable and was reproducibly varied with heating current. However, its resistance became very unstable above 1400℃. After experienced the unstable state, a surface of Pt specimen has changed to gray powder. In view of the occurrence of a chemical reaction between Pt and B at pressure of 30 kbar and temperature of 500℃ as reported by Whitney and Gase,[54] the abnormality in Pt in our experiment would be the same reaction of Pt with isolated B in BN. This is the reason why the quenching temperature was restricted below 1350℃ in the present experiment.

3. 4. Conclusion

Pt wires were successfully quenched under high pressures up to 100 kbar in making use of a solid BN as pressure transmitting and cooling medium. A new high pressure cell which permits four-probe electrical resistance measurements was developed. High pressures could be generated with fairly good reproducibility, and an accurate electrical resistivity of a specimen has been measured without regards to contact resistance and sample distortion.

Cooling rate in this experiment was about 3 to 12×10^4℃/sec which is very close to the maximum cooling rate reported by Jackson for Pt quenching in water. Moreover, quenching within a solid had the advantage of the higher rate at initial stage of cooling. From the measurement of quenched-in resistivity the following results were obtained; $\Delta E_f=1.52$ eV at 0 kbar, $\Delta H_f=1.84$ eV at 30 kbar, and $\Delta V_f=1.18\times10^{-23}$ cm³/atom (0.77 atomic volume) at 1100℃.

The present method of quenching in solid should be useful for the vacancy study giving informations on the lattice relaxation about vacancies at very high pressure and high temperature.

Chapter IV. Measurements of Lattice Compression by High Pressure X-ray Diffractometry[55-57]

4. 1. Introduction

Since the pressure-volume relations for many metals were originally measured by Bridgman,[58,59] a variety of experimental techniques have been developed for the determination of the pressure-volume relations under high pressures: (a) piston=cylinder method; (b) shock-wave measurement; (c) ultra-sonic measurement; (d) X-ray diffraction method. In order to check these existing compression data, recently, Vaidya *et al.*[60-62] have made careful measurements of volume up to 45 kbar using the piston-cylinder technique. These experimental results were not necessarily in agreement with each other and there were some inconsistency among these various experimental data.

As for the X-ray diffraction under high pressure many improvements of the experimental technique and precision have been made recently in combination with the newly developed high pressure generators by Jamieson,[63-65] Hall,[66] Drickamer,[67] Bassett[68,69] and so on.

There are some difficulties,[70] however, in the X-ray diffraction under high pressure such as; i) Since experiment stands in need of penetrative X-ray source having a short wave length such as Mo-K_α or Ag-K_α, the available reflections are apt to concentrate within the low-angle region. ii) Limitation such as the size of the pressure cell or the geometrical arrangement of the high pressure apparatus makes an efficient X-ray focusing method hard to apply. iii) Off-centering of the sample and the geometrical mis-alignment of the X-ray optical system are, though very slight, usually inevitable in the course of loading. iv) A reflection profile should be affected by lattice defects or shear stresses due to plastic deformation of the sample in the solid pressure-transmitting medium. All of these difficulties deteriorate to some extent the precision of the experiment in comparison with the diffraction at an ordinary pressure.

The present study is concerned with the precise measurement of the lattice compression of Al, Si and Al-Si alloys under high pressure up to 90 kbar made by the combination of cubic anvil press, rotating-target type X-ray source, and goniometer. Several improvements on the method of correction for the systematic or non-systematic errors caused by the above-mentioned difficulties have been made aiming at the higher precision.

A main part of the present paper consists of description of the details of the experimental procedure along with the method of error correction. Then the data obtained are discussed in comparison with the existing experimental data and calculations by the pseudopotential method.[71] Also is included the discussion of peak shifts due to stacking faults in Al-Si solid-solution and of some differences between the lattice contraction in the solid pressure-transmitting medium and that in the hydrostatic environment.

4. 2. Experimental apparatus and procedures

4. 2. 1. High pressure apparatus and X-ray diffractometer

High pressure is generated within a $6\times6\times6$ mm^3 sample cell compressed by a hydraulic press-driven cubic anvil apparatus, which is the same type of Inoue and

Asada.[72] The bottom hydraulic ram of this press is equipped with a table, on which the whole X-ray system, the X-ray source with vacuum system and the goniometer, is mounted. No relative motion between these optical units can, therefore, occur even by the vertical motion of the hydraulic ram. Also the relative vertical distance between the ram and the mounting table is micro-adjustable within ± 10 mm. This serves well not only to correct the vertical displacement of the sample during compression, but also to change at will the part of the specimen irradiated by X-ray without readjusting the whole X-ray optical system. In Fig. 19 is shown the arrangement of the X-ray optical system and the anvil unit.

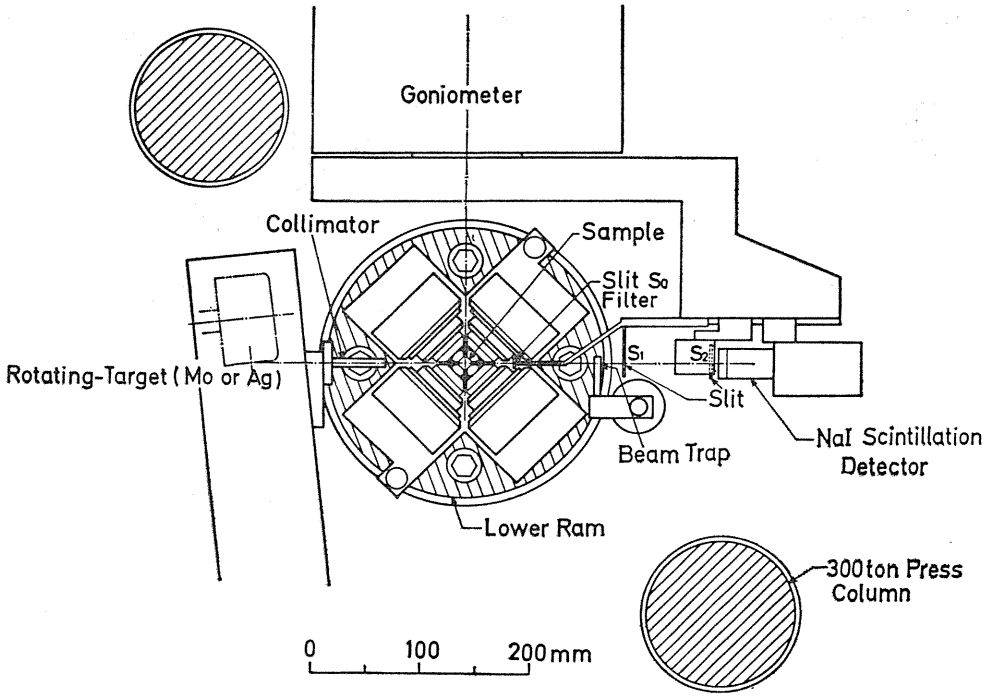

Fig. 19. Cubic anvil press equipped with high power X-ray source and goniometer.

The X-ray source is a rotating-target type generator of which maximum capacity is 12 kW. As the targets both of Mo at 60 kV-200 mA max. and Ag at 60 kV-150 mA max. have been used. From the forcal area 0.5×10 mm² imaged on this target a point-focus X-ray beam having an effective area 0.5×1 mm² was taken out. This X-ray beam, after being choked through a 0.3 mm-wide slit-type collimator, penetrates the gasket formed between the side anvils and impinges the specimen. The diffracted X-rays proceed through the anvil gap on the opposite side, and passes through the slit, S_0, to proof background, the filter to eliminate the K_β radiation and the receiving slit, S_1 or S_2, finally reaching to the NaI scintillation counter. Figure 20 shows the relative positions of these collimators and receiving slits.

The transmission powder method was employed in which due to the geometry of the anvil ends the measurable range of the diffraction angle 2θ was limited to $\pm 35°$. Over this range with precision of $\pm 0.004°$ the goniometer having only 2θ axis scans

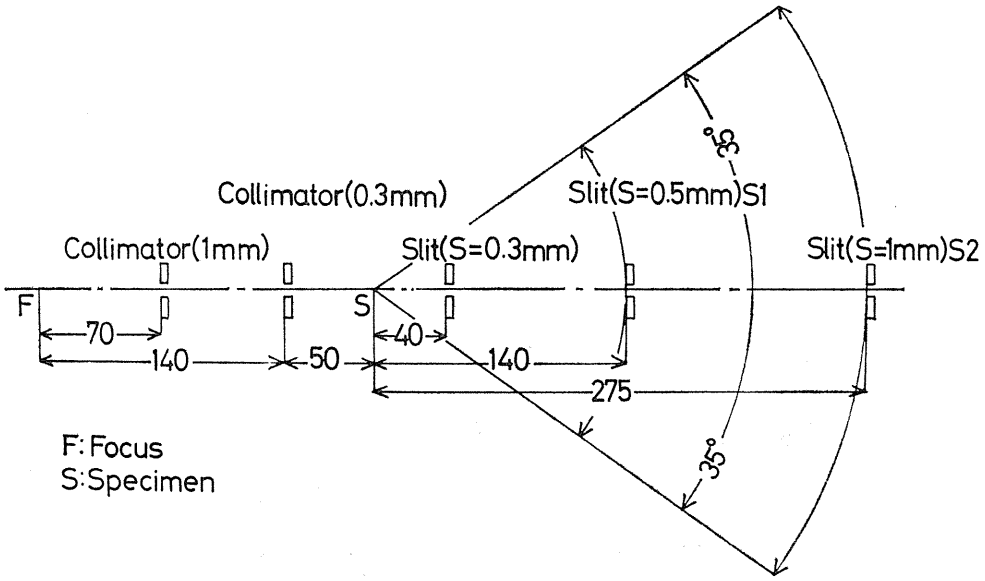

Fig. 20. Arrangement of collimator and slits in X-ray optical system.

continuously at a rate of 1° to 1°/32 per minute or scans stepwise at intervals 0.01 to 0.2°.

4. 2. 2. Sample and pressure cell

Samples on which the lattice compression measurements have been made were such as, a pure Al (99.999%), a pure Si (99.999%), two Al-Si alloys, *i.e.*, Al-3.7% Si solid-solution and Al-15%Si having two phases. NaCl (99.99% standard reagent) was used as the calibrant for the pressure determination.

The pure Al specimen was cut out from a cast block and then its crystal grains were deformed plastically and made fine. The powder specimens of Si and NaCl were formed into a disk of 13 mm o.d., 0.5 to 0.7 mm thick by pressing at about 5 kbar, and then were shaped into the fixed dimension $3\times2\times0.5$ mm^3. Before submitting to the experiment Si specimen was annealed in vacuum at 650℃ for 1.5 h, and Al specimen at 200℃ for 1 h.

Under ordinary pressure the Al-Si binary system is known as a typical alloy forming a partial solid solution A solid solubility of Si in Al is 1.6% at 577℃. but at room temperature practically no solubility appears on both sides of the constituents, showing only a mixed structure of Al and Si [27] At high pressure, however, the solid-solubility limit is much enhanced to the extent of 9% 660℃ at 28 kbar and more than 15% at 54 kbar, and these Si-supersaturated solid solutions could be quenched to the ordinary pressure and temperature as fully mentioned at chapter III. Sample of the Al-3.7%Si alloy was one obtained by quenching the solid solution at 500℃, 28 kbar. Thus at ordinary state the material is a Si-supersaturated solid solution showing no diffraction line of Si. Sample of the Al-15% Si alloy is a cast alloy, annealed in vacuum at 400℃ for 3 h to obtain a two-phase structure of Al and Si, on each of which the lattice contraction was measured.

The pressure cell was made of an amorphous boron mixed with 67 wt% polyester

resin as the hardener. It is obvious that the lesser is the resin quantity, the higher is decreased the absorption of X-rays and the S.N. ratio of diffraction pattern. However it was found difficult to construct the pressure cell with less resin. The pressure cell is a cube whose edge is 9 mm.

As shown in Fig. 21a the pressure cell was cut along its diagonal face into two pieces between which the sample material and the calibrant NaCl were buried. In the pressure cell the sample and the calibrant were not mixed, but were located as shown in the figure for the benefit of changing the irradiated part of the sample. This arrangement works well for preventing the interference between the reflections from the two materials. This is especially efficacious for the materials which have similar crystal structures and lattice constants, such as Si and NaCl.

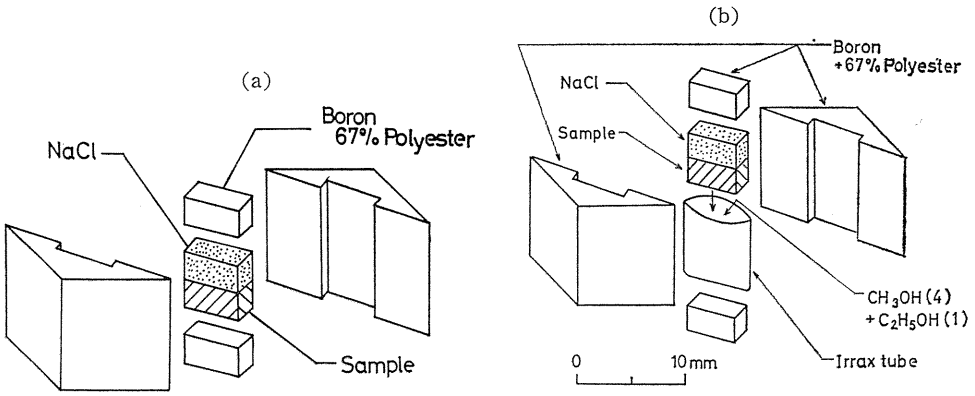

Fig. 21. Configuration of the sample cell for high pressure X-ray diffractometry.
(a) Solid pressure-transmitting medium, (b) Liquid pressure-transmitting medium.

In the present experiments two kinds of compression measurements have been performed. One was the usual method in the plain solid medium, and the other was by means of the hydrostatic pressure as shown in Fig. 21b. In the latter experiment the specimen and NaCl pellets prepared above were enclosed along with the liquid pressure-transmitting medium, 1 : 4 mixture of ethanol and methanol, in a polyethylene tube, 3 mm o.d., which was buried in the pressure cell. This liquid medium is reported to keep the hydrostaticity over a pressure of 100 kbar at room temperature by Piermarini *et al.*.[73,74]

4. 2. 3. Experimental procedures

After setting the pressure cell in the very center of the anvil apparatus, the press load was increased at a rate of 1 to 1. 5 ton/min up to a fixed load on which thereafter it was kept constant. The completely collimated X-ray system is mounted on the bottom hydraulic ram, so that relative motion between the X-ray system and the anvil apparatus can not occur even by the vertical motion of the hydraulic ram during the loading. In addition, the vertical shift of the sample position due to deformation of the pressure cell was adjusted so as to make the diffracted beam strongest. A practice of such a position adjustment shouid be needed for every reflection from the sample which has preferred orientation, because the equivalent center of the diffraction is movable in every reflection.

First the whole diffraction pattern was checked by a continuous scanning at a rate of 1°/min over −35° to +35°. Then a step-scanning of a time interval 4 to 40 sec and an angular interval 0.05° has been performed in order to determine the reflection profile in detail. The slits S_1 and S_2 in Fig. 20 are the provision for correcting the possible shift of the sample in the direction of the X-ray beam, Although details will be given in the next paragraph, the scanning was performed in twice for each reflection by inserting these slits alternately.

To assign the diffraction angle $2\theta_m$, the remnant given by subtracting the background from the step-scanned profile was averaged with weights as

$$2\theta_m = \sum_i 2\theta_i (N_i - N_b) / \sum_i (N_i - N_b), \tag{10}$$

where N_i is a counting rate at $2\theta_i$, N_b is a background. This process is applicable to non-symmetric diffraction profile. Then the weighted average of the wavelength of $K_{\alpha 1}$ and $K_{\alpha 2}$ radiation was used as the pertaining wave-length of the X-ray. The diffraction angles measured on both sides of the X-ray beam have been added up and the lattice spacing was obtained from the diameter 4θ of the Debye ring after making the error correction due to the off-centering of the sample. Lattice spacings thus obtained have been extrapolated to the diffraction angle of $\theta = 45°$ in order to obtain the correct value.

4. 2. 4. Error correction

4. 2. 4. 1. Correction of error due to off-centering of sample

It seems inevitable in the high pressure experiment that the sample is apt to be off the center of the goniometer. From the constitution basis of the anvil apparatus, it is difficult to rotate the sample around the center of the goniometer. Thus, since the direction of the sample against the incident X-ray beam is fixed, the crystal grains which contribute to the diffraction are not the same for different reflections. If there is no preferred orientation in the sample, the magnitude of the off-centering should be unrelated to the diffraction angle giving only a systematic error against the whole reflections of the same sample. When the sample has a preferred orientation, however, the equivalent center of diffraction is changed with every reflection leading to a non-systematic error.

In the direction perpendicular to the incident X-ray beam, the off-centering of the sample must be smaller than the beam section, and moreover the errors under such a condition are easily corrected. Among these the systematic error can be corrected by measuring the diameter 4θ of Debye ring, and the non-systematic one by micro-adjusting the irradiated part so as to make the intensity maximum for each reflection as mentioned in the section 4. 2. 3.

As for the off-centering of the sample along the incident beam direction, there is a correction in which an extrapolation to $2\theta = 180°$ based on the Nelson-Riley's equation is made. However, this principle is applicable only to the systematic errors. Moreover, when the detectable reflections are concentrated within a range of the small diffraction angles, they can not effectively be corrected.

In the present experiment, therefore, the newly-devised procedures are applied; the diffraction angle was measured in twice by means of exchanging the slits for each reflection, and then the non-systematic errors due to the off-centering of sample are corrected in the following way. Denote the diffraction angle by 2θ in Fig. 22. When there is a shift, X, of the sample in the beam direction, the angular

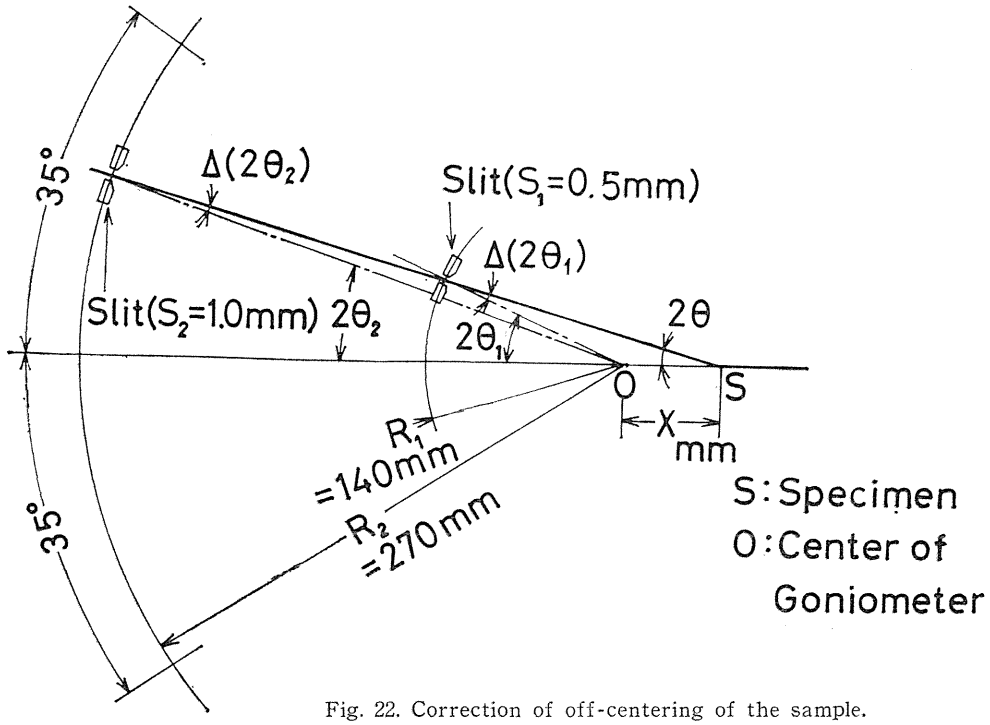

Fig. 22. Correction of off-centering of the sample.

change, $\Delta(2\theta)$, is given by,

$$\Delta(2\theta)=(X/R)\sin 2\theta \tag{11}$$

where R is the distance between the center of the goniometer and the slit. The angular change $\Delta(2\theta)$ is decreased with increasing R and vanishes when $R=\infty$. For the slits, S_1 at $R=R_1$ and S_2 at $R=R_2$, the following two relations are obtained by eq. (11),

$$\begin{aligned}\Delta(2\theta_1)&=(X/R_1)\sin 2\theta,\\ \Delta(2\theta_2)&=(X/R_2)\sin 2\theta.\end{aligned} \tag{12}$$

From Fig. 22. another relation

$$\Delta(2\theta_2)-\Delta(2\theta_1)=2\theta_2-2\theta_1 \tag{13}$$

is obtained. From eqs. (12) and (13),

$$\Delta(2\theta_2)=(2\theta_2-2\theta_1)/(1-R_2/R_1). \tag{14}$$

Thus,

$$\begin{aligned}2\theta&=2\theta_2-\Delta(2\theta_2)\\ &=2\theta_2-(2\theta_2-2\theta_1)/(1-R_2/R_1),\end{aligned} \tag{15}$$

which gives a relationship between the true diffraction angle 2θ and the angles, $2\theta_1$ measured by slit S_1 and $2\theta_2$ by S_2. In the present work, two slits, 0.5mm×6.5mm at $R_1=140$mm as S_1 and 1mm×13mm at $R_2=275$mm as S_2, have been provided, considering their angular resolutions. Similar correction could be found in the camera method by the use of two parallel films.[75]

4. 2. 4. 2. Correction of error due to the truncation of the diffracted Debye cone

As mentioned before, the incident and diffracted X-rays pass through the very narrow gaps between the side anvils in this apparatus. If there is any non-uniformity in the displacements of anvils in the course of the loading, however, the incident X-ray beam is not in-plane with the diffracted X-rays truncated by the anvils. This gives rise to the shift of the Debye ring, so that the 2θ is measured smaller than the true value. The errors due to such cause are systematic for each reflection, and analyzed and corrected in the following way.

The cone formed by diffracted X-rays is shown in Fig. 23; the most part of it is truncated by the anvils. In this figure the origin is located at the intersection of the X-ray beam and the orbit of receiving slit, and the z-, y- and x-axes are taken in the direction of the X-ray beam, the sweeping direction of the slit and the direction perpendicular to the former two, respectively. Thus the equation of intersecting line formed by the Debye cone and the orbital cylinder of the receiving slit is expressed as follows,

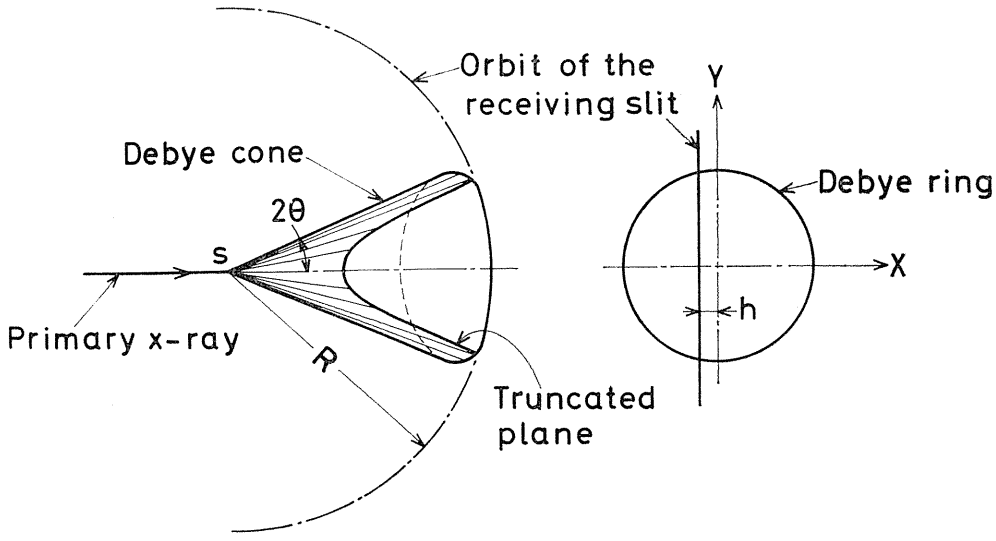

Fig. 23. Debye cone and orbit of receiving slit.

$$x^2+(1+\tan 2\theta)\,y^2=R^2\tan^2 2\theta \tag{16}$$

from which y is evaluated for the shift x. The difference between y and y_0 for $x=h$ and $x=0$ respectively is also translated to $\Delta(2\theta)$, the error of 2θ, in term of $\Delta\theta$ as follows,

$$\Delta\theta = -(h^2/4R^2)\cot 2\theta. \tag{17}$$

There is another relationship between the relative error of the lattice constant $\Delta a/a$ deduced from the Bragg's diffraction condition and the error in the angle measurement $\Delta\theta$ such as,

$$\Delta a/a = -\cot\theta \cdot \Delta\theta. \tag{18}$$

Thus from eqs. (17) and (18) an equation giving the relative error of the lattice constant is obtained as follows,

$$\Delta a/a = (h^2/8R^2)(1/\tan^2\theta - 1), \tag{19}$$

in which $\Delta a/a$ vanishes for $\theta = 45°$.

There has been an extrapolation method (Umbrella effect[76]) in Debye-photography of a rod sample at an ordinary powder camera. The functional type of eq. (19) is similar to that. By using eq. (19) as a regression function in the present study, a and $(1/\tan^2\theta\text{-}1)$ for various θ have been plotted. The value of a obtainable by extrapolating this plot to $\theta = 45°$ by means of the least square method has been taken as the value of the lattice constant.

4. 3. Results and Discussions

4. 3. 1. Lattice compression

The X-ray diffraction measurements were made at several points of load up to 200 ton. To confirm the reproducibility, these measurements were carried out in several times for Al and Si. The ambient pressures have been determined from the contraction of the NaCl lattice using Decker's calculated values.[12] In the case of using Ag-K_α as the X-ray source, six reflections, (200), (220), (222), (400), (420) and (422) were used for determining the lattice parameter of NaCl. The reflections of Al and Si were (111), (200), (220), (311) and (222), and (111), (220), (311), (400) and (331), respectively. All the experiments were performed at controlled room temperature of 20 to 23 ℃.

4. 3. 1. 1. Aluminum

There was no significant difference among the lattice compression of the pure Al, Al-15%Si alloy matrix and Al-3.7%Si solid solution by the solid pressure-transmitting medium. The effect on the compressibility of Al due to the alloying of Si was so small that it is not detectable by the present measurements. In Fig. 24 are shown these results along with the results of pure Al in the liquid medium. As shown in this figure there is no difference also between the lattice contraction in the solid medium and in the liquid medium. Bulk compression data,[58, 60] shock wave data[77] and calculated values by the present authors[71] are shown in the same figure. The Bridgman's data were corrected as mentioned at a later section, because his data had been obtained in 1940's, a pressure scale at that time had been known to be different from that currently accepted.[78] The present experimental values show fairly good agreement with the calculated values. As for the comparison with the other bulk compression experiments, the present results give slightly more compressible values than those in the bulk compression.

To obtain the bulk modulus B_0 and its pressure derivative B_0', the present

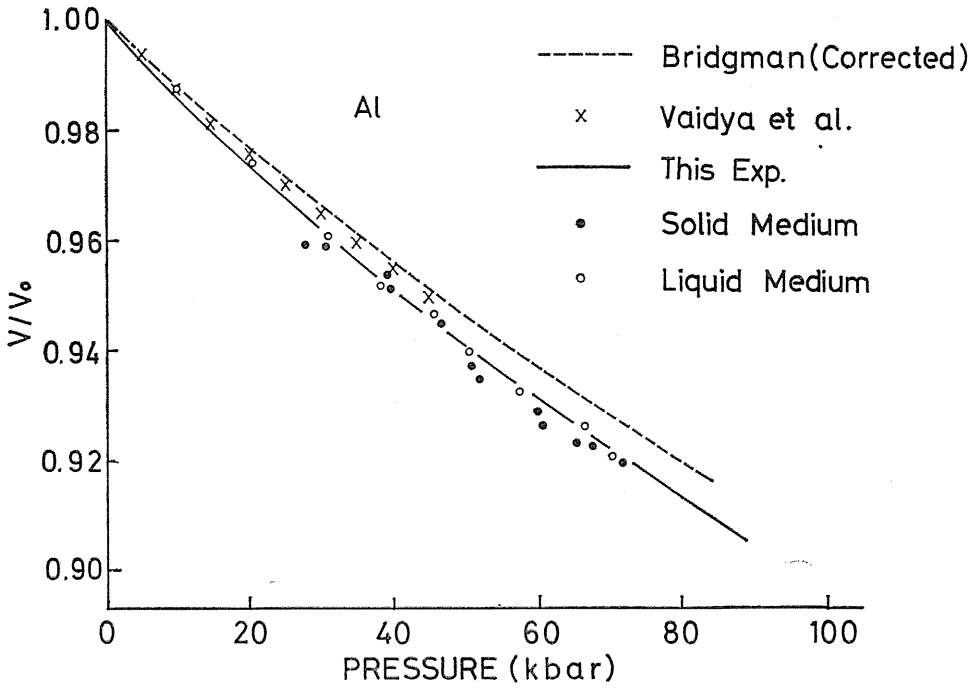

Fig. 24. Compression of Al.

experimental values have been fitted to Murnaghan's equation of state,

$$P=(B_0/B_0')[(V_0/V)^{B_0'}-1] \tag{20}$$

by the method of least squares. The results are

$B_0=710$ kbar, $B_0'=4.0$ (solid medium)

and

$B_0=730$ kbar, $B_0'=4.1$ (liquid medium).

Table 10 shows a comparison of these values of B_0 and B_0' with those given by other authors.

Table 10. Bulk modulus B_0 and B_0' for Al

Author		Method	Pressure range (kbar)	B_0 (kbar)	B_0'
Bridgman[58]	(1948)	Piston-cylinder	85	799.1	4.32
Schmunk *et al.*[79]	(1968)	Ultra-sonic	2	760	4.42
Vaidya *et al.*[60]	(1970)	Piston-cylinder	45	781.4	4.14
Senoo *et al.*[56]	(1976)	X-ray (Solid medium)	80	710	4.0
Senoo *et al.*[57]	(1976)	X-ray (Liquid medium)	80	730	4.1

4. 3. 1. 2. Silicon

In Fig. 25 are shown the results obtained for pure Si and precipitated Si in Al-15%Si alloy, and for pure Si using a liquid pressure transmitting medium. As seen from the figure a considerable difference exists between the measurements by the solid medium and by the liquid medium. Compared with the bulk measurements by means of the piston-cylinder apparatus, the present results obtained by the liquid medium are fairly consistent with the data of Vaidya and Kennedy[62] up to 45 kbar and with the calculated values by the present authors.[71] While the considerable discrepancy exists between the lattice compression data by solid medium and the Bridgman's bulk compression data, even though compared with those by liquid medium, the discrepancy which is still a half value of the former can be found appreciably above the pressure of 50 kbar. This discrepancy is increased with pressure, and is about 0.02 in V/V_0 at pressure of 80 kbar.

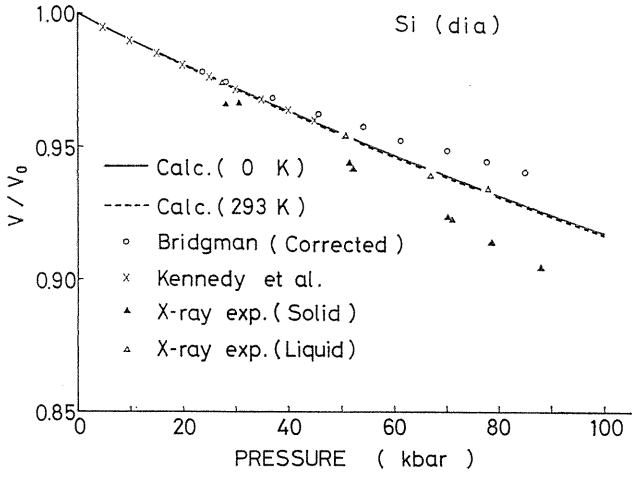

Fig. 25. Compression of Si.

The bulk modulus B_0 and its pressure derivative B_0' of Si are

$$B_0=810 \text{ kbar}, \quad B_0'=1.3 \qquad \text{(solid medium)}$$

and

$$B_0=960 \text{ kbar}, \quad B_0=3.9 \qquad \text{(liquid medium)}.$$

Table 11 shows a comparison of these values of B_0 and B_0' with those given by other authors.

In the experiments of Vaidya and Kennedy, the compression was made under a sufficiently hydrostatic condition since the specimen is contained by a soft material such as indium. The values of these two kinds of experiments and the present ones by the liquid medium are fairly consistent with each other. Thus measurements under hydrostatic pressure could give the same results in spite of the difference in apparatuses and methods.

On the other hand it is considered in the Bridgman's experiments that bare specimen was directly inserted into the cylinder and suffered substantial deformation in the course of loading similar to that in the present experiments by the solid

Table 11. Bulk modulus B_0 and B_0' for Si.

Author		Method	Pressure range (kbar)	B_0 (kbar)	B_0'
Bridgman[58]	(1948)	Piston-cylinder	85	920	12.3
McSkimin *et al.*[80]	(1964)	Ultra-sonic	2	978.8	4.24
Vaidya *et al.*[62]	(1972)	Piston-cylinder	45	1007.5	4.72
Senoo *et al.*[55]	(1975)	X-ray (Solid medium)	90	810	1.3
Senoo *et al.*[56]	(1976)	X-ray (Liquid medium)	80	960	3.9

medium. When the specimen was plastically deformed, a substantial discrepancy might be risen between the bulk and X-ray measurements. Compare these results under unhydrostatic pressure with the results under hydrostatic pressure, it is noticed that the directions of the deviations from the hydrostatic measurements are just opposite to each other, *i. e.*, the bulk measurements and the X-ray measurements give incompressible and compressible data, respectively. Such substantial discrepancy between the bulk and lattice compression under unhydrostatic pressure can not be found in Ge which has the same crystal structure and properties as Si.[55] Though the causes of the discrepancy could not be clarified in the present experiments, it should be considered that the experimental results in solid medium are more or less affected by the complex shear stresses and lattice defects introduced by the heavy deformation of the specimen.

Recently Singh and Kennedy[81] analyzed a uniaxial stress component in Si powder strongly deformed under uniaxial loading, using a Bridgman anvil type high-pressure X-ray camera. They pointed out that beside a hydrostatic component the considerably large uniaxial stress component existed especially in Si powder.

4. 3. 2. Accuracy

To discuss an accuracy of measurements and an effect of error corrections, measurements of lattice compressions on an Al-15%Si alloy are described as an example. The X-ray diffraction measurements, using Mo-K_α in power of 56 kV, 150 mA, were performed at the loads of 0, 50, 100 and 150 ton. For all diffraction lines correction was made for the off-centering of the sample, and then the extrapolation method were applied as mentioned in section 4. 2. 4. The effects of such corrections in the measurements of NaCl at 0 and 150 ton are shown in Fig. 26. In the figure solid circles represent lattice constant calculated from observed data and open circles the values corrected. The dotted line shows a mean of raw data and its value is (5.6417 ± 0.0017) Å at 0 ton or (5.3016 ± 0.0034) Å at 150 ton. The regression line to eq. (19) is shown as a solid line, and the extrapolated value is (5.6347 ± 0.0007) Å at 0 ton and (5.2917 ± 0.0015) Å at 150 ton. A standard error of the mean value or the extrapolated value given from scatters of the data points is shown. Corrections certainly seem to be valid to make the error less than a half. The relative error in the lattice constant measurements in the present experiment is about ±0.0002, which was one fifth of the error in a usual high pressure X-ray camera.

In Fig. 24 or Fig. 25 the errors due to the scatters only were ±1 kbar in the pressure and 0.001 in V/V_0 at 60 kbar, where Murnaghan's equation of state is used as a regression curve, becomes about 0.002 in the solid medium or 0.001 in

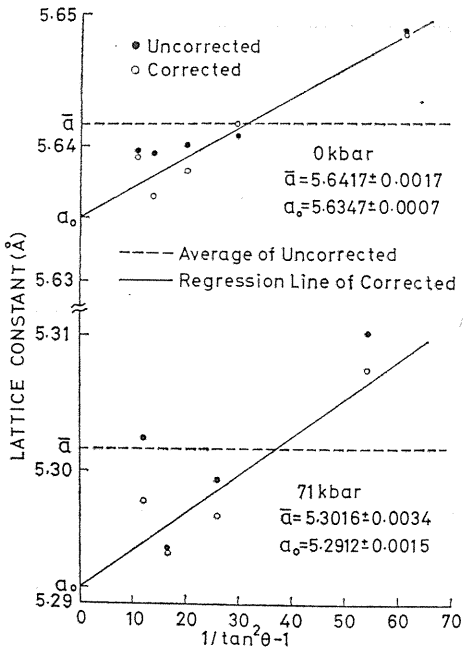

Fig. 26. Results of correction of the off-centering effect and extrapolation of the lattice constant of NaCl.

the liquid medium, respectively. The error could be reduced to approximately half the value in the solid medium by using the liquid pressure-transmitting medium.

The ambient pressure in the cell was determined by lattice contraction of NaCl embedded with the specimen, referring to the values calculated by Decker.[12] The accuracy of the pressure determination due to the error in the measurement of lattice contraction is about ± 1 kbar as mentioned above. In addition to this, however, error in the equation of state of NaCl and error due to inhomogeneity of pressure distribution in the cell should be included. Decker's error estimation in his calculation is 1 % up to 50 kbar and 1.5 % up to 100 kbar.

To check the pressure distribution in the solid pressure-transmitting medium, the pressure at the center and at the place 1 mm from the center were measured by making use of the pressure cell in which only NaCl is embedded. The results were (43.2 ± 1.0) kbar at the center and (44.4 ± 1.0) kbar at 1 mm from the center under the load of 80 ton, and (66.4 ± 1.5) kbar and (70.2 ± 1.3) kbar under 150 ton, respectively. However, NaCl and the specimen have been symmetrically placed with respect to the center of the cell, so that these pressure difference seems to be diminished. The difference is then estimated to be within ± 2 kbar at the pressure in excess of 50 kbar. Taking into account the all kinds of error, the value of ± 2 kbar up to 50 kbar and ± 4 kbar around 70 kbar were consequently obtained as the error of the ambient pressure.

As for another problem in high pressure X-ray diffraction, Olinger and Jamieson[82] and Sato, Akimoto and Inoue[83] pointed out that due to the difference in compressibilities of respective materials an internal stress difference can be generated in a cell when a mixture of sample material and pressure calibrant is loaded into the cell. In our experiment, however, this effect was avoided by the cell arrangement in which the sample and the calibrant were separated.

4. 3. 3. Correction of the peak shifts due to stacking faults

The specimen in the solid pressure-transmitting medium is deformed in the course of loading, so that various defects are inevitably introduced in the specimen. In cold-worked fcc metals, it is generally noticed that peak position and breadth of the diffraction line are substantially affected by stacking faults.[84, 85] The peak shifts due to the stacking faults are corrected in the experiments of Al-3.7%Si solid solution, and the effects on the accuracy of lattice constant measurements are discussed in this section.

Following Paterson,[86] Warren,[84] Warren and Warekois,[87] a relative change in the lattice parameter, $\Delta a/a$, due to stacking faults in a fcc metal, which is dependent on a reflection index hkl, is given by

$$(\Delta a/a)_{hkl}=\alpha\cdot G_{hkl} \tag{21}$$

where α is the stacking fault probability, and

$$G_{hkl}=-(\sqrt{3}/4\pi)[\textstyle\sum_b(\pm)(h+k+l)/(h^2+k^2+l^2)(u+b)] \tag{22}$$

b is the number of components of the reflections which are affected by stacking faults (*i. e.* $h+k+l=3N\pm1$, where N is an integer) and u the number of components for which $h+k+l=3N$ not affected by stacking faults.

The lattice constant of each reflection was corrected by means of this relation as a function of the stacking fault probability, and then α was determined so as to minimize the sum of the square of the residual, σ^2, when the corrected values were

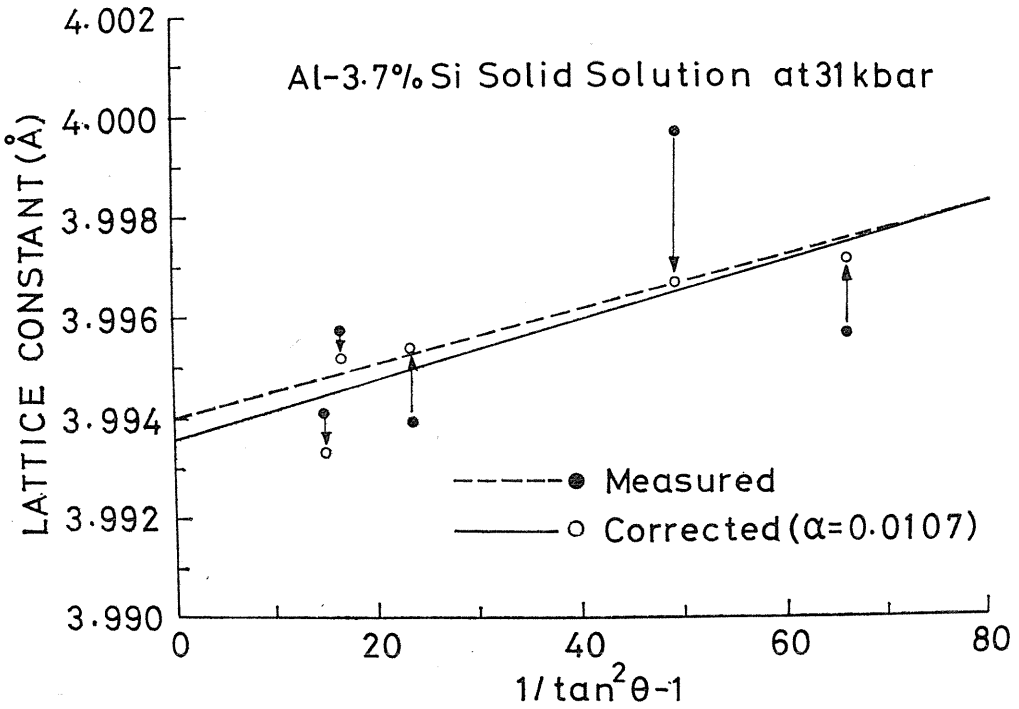

Fig. 27. Correction of peak shifts due to stacking faults.

Table 12. Stacking fault probability and its error correction in solid solution of Al-3.7 %Si alloy.

Pressure (kbar)	Measured		Corrected		Stacking Fault Probability (%)
	a_0(Å)	$\sigma^2(10^{-8})$	a_0(Å)	$\sigma^2(10^{-8})$	
0	4.0497	25	4.0497	24	0.04
31	3.9940	518	3.9936	67	1.07
51	3.9637	320	3.9633	9	0.90
66	3.9436	92	3.9436	1	0.40
0	4.0502	26	4.0502	26	0.01>

regressed to eq. (19). In Fig. 27 are shown the experimental results under the load of 50 ton as an example. The lattice constant corrected with $\alpha=0.0107$ (denoted by circle points) gave the least value of σ^2, 6.7×10^{-7}, while σ^2 was 5.18×10^{-6} for uncorrected values (denoted by black points). These results are summarized in Table 12. It is shown in the table that the intrinsic stacking faults was included in the Al-3.7%Si solid solution under high pressure, and that the standard deviation in lattice constant could be reduced to one third by making the correction of the peak shifts. The extrapolated value of the lattice constant has not been, however, so much affected.

It can be found that the stacking fault probability is abruptly increased in the initial stage of the loading, and then gradually decreased with increasing pressure, being almost zero after the compression. However, it is hard to assume that the peak shifts under high pressure are entirely due to stacking faults. When the stresses in the sample will be analyzed by making use of the diffraction peak shifts as proposed by Singh and Kennedy,[81] then, such influences due to the faults should be taken into account. This analysis may offer the means to study lattice defects under pressure. On the other hand the systematic peak shifts in the other specimens, *i.e.*, pure Al, Al-15%Si alloy matrix, pure Si and NaCl, were not appreciable.

4. 3. 4. Correction on Bridgman's Pressure scale

Bridgman's measurements of the compressibility of solids by means of the

Table 13. Correction of Bridgman's data.

Pressure		V/V_0	
Original	Corrected	Al	Si
25,000 kg/cm^2	23.6 kbar	0.970	0.978
30,000	28.1	0.966	0.974
40,000	37.0	0.958	0.968
50,000	45.6	0.951	0.962
60,000	54.0	0.944	0.957
70,000	62.1	0.937	0.952
80,000	70.0	0.929	0.948
90,000	77.6	0.922	0.944
100,000	85.0	0.915	0.940

double stage piston-cylinder apparatus is our sole source of bulk *PVT* data up to 100 kbar, and have often referred up to the present. The experiments was, however, performed in 1940's, and it has been appeared nowadays that the pressure scale at that time should be considerably different from one at the present time.

This difference can be estimated by making use of the transformation pressure of the pressure sensitive metals, *i. e.*, Tl, Cs, Ba and Bi, in Bridgman's measurements and the best values recently published by Decker.[7,8] To obtain the correction for Bridgman's compression data, the discrepancies of the transformation pressure on these metals was fitted to a quadratic curve by means of the least square method. In Table 13 are shown the corrected values of pressure translated to the unit of kbar with the compression data of Al and Si.

4. 4. Conclusion

In making use of a cubic anvil press equipped with a rotating-target type X-ray generator and a goniometer, lattice compressions in Al, Si and Al-Si alloys were accurately measured up to 90 kbar by improving the experimental precision. Especially to avoid an inhomogeneity of pressure distribution in a cell and a deformation of specimen during loading, a liquid mixture of ethanol and methanol was used as a pressure-transmitting medium.

The results obtained by such newly-devised experiments are as follows;

1) Correction of errors due to off-centering of a sample and misalignment of an X-ray optical system was successfully established. Then the lattice constant could be measured under high pressure with the standard error of ± 0.02 %, which was one fifth of the error in a usual high pressure X-ray diffraction using camera. The total accuracy in determining the ambient pressure was ± 2 to 4 kbar, and that in determining the volumetric ratio, V/V_0, was ± 0.001.

2) No difference was found between the lattice compression of Al in the solid medium and in the liquid medium. The compressibility of pure Al obtained in the present experiments shows fairly good agreement with the calculation by the pseudopotential method, and is slightly larger than that in the bulk measurements.

3) The considerable difference in the lattice compression of Si could be found between the experiments using the solid medium and liquid medium. The results in the liquid medium were fairly consistent with the bulk measurements of Vaidya and Kennedy rather than those of Bridgman, and agreed very well with the calculated values by the pseudopotential method.

4) Many stacking faults were contained in Al-3.7%Si solid soution under high pressure, and the standard error in the measurement of lattice parameter was fairly reduced by means of correcting the peak shifts due to these faults.

References

1) H. Mii, I. Fujishiro and T. Nomura: *Les Proprietes Physiques des Solides sous Pression* (CNRS, Paris, 1970) p. 441.
2) H. Mii, I. Fujishiro, M. Senoo and K. Ogawa: High Temperatures High Pressures, **5** (1973) 155.
3) H. Mii and I. Fujishiro: Nihon Kikai Gakkai-shi, **72** (1969) 476 [in Japanese].
4) H. Mii: Nihon Kinzoku Gakkai-ho, **10** (1971) 382 [in Japanese].
5) H. Mii and I. Fujishiro: Nihon Kikai Gakkai-shi, **76** (1973) 1099 [in Japanese].

6) E. C. Lloyd: *Accurate Characterization of the High-Pressure Environment* (US Nat. Bur. Stands., Washington, 1971) NBS Special Publication No. 326.
7) H. G. Drickamer: Rev. sci. Instrum., **41** (1970) 1667.
8) L. F. Vereshchagin, A. A. Semerchan, N. N. Kuzin and Yu. A. Sadkov: Soviet Phys. Doklady, **15** (1970)292.
9) R. N. Jeffery, J. D. Barnett, H. B. Vanfleet and H. T. Hall: J. appl. Phys., **37** (1966)3172.
10) D. L. Decker: J. appl Phys., **36** (1965) 157.
11) D. L. Decker: J. appl. Phys., **37** (1966) 5012.
12) D. L. Decker: J. appl. Phys., **42** (1971)3239.
13) T. Takahashi, H. K. Mao and W. A. Bassett: Science, **165** (1969) 1352.
14) H. K. Mao, T. Takahashi and W. A. Bassett: *Carnegie Institution Yearbook* (Carnegie Institution, Washington, 1970) Vol. 68, p.251.
15) T. Yagi and S. Akimoto: J. appl. Phys., **47** (1976) 3350.
16) H. Mii, I. Fujishiro and M. Senoo: Rep. of Toyoda Phys. Chem. Res Inst., **22** (1969) 33 [in Japanese].
17) W. Stark and G. Jura: ASME Paper, 64-WA/PT-28 (1964).
18) A. Giardini and G. Samara: ASME Paper, 64-WA/PT-10 (1964).
19) H. T. Hall: *Accurate Characterization of the High-Pressure Environment*, ed. by E. C. Lloyd (US Nat. Bur. Stands., Washington, 1971) NBS Special Publication No. 326, p. 303.
20) M. H. Rice, R. G. McQueen and J. M. Walsh: *Solid State Physics*, ed. by F. Seitz and D. Turnbull (Academic Press, New York, 1958) Vol. 6, p. 1.
21) P. W. Bridgman: Proc. Amer. Acad. Arts Sci., **71** (1937) 387.
22) I. Fujishiro, H. Mii, M. Senoo and M. Akao: J. Soc. Material Sci. Japan, **20** (1971) 952 [in Japanese].
23) H. Mii, M. Senoo and I. Fujishiro: Japan. J. appl. Phys., **15** (1976) 777.
24) H. Mii and I. Fujishiro: Nihon Kessyo Gakkai-shi, **16** (1974) 341 [in Japanese].
25) T. Kaneko and N. Miura: Nihon Kinzoku Gakkai-ho, 8 (1969) 473 [in Japanese].
26) T. Kaneko and N. Miura: Nihon Kinzoku Gakkai-ho, **9** (1970) 231 [in Japanese].
27) M. Hansen: *Constitution of Binary Alloys* (McGraw Hill, New York, 1958) p. 132.
28) H. S. Rosenbaum and D. Turnbull: Acta metallurgica **6** (1958) 653.
29) H. S. Rosenbaum and D. Turnbull: Acta metallurgica **7** (1959) 664.
30) E. Ozawa and H. Kimura: Acta metallurgica 18 (1970) 995.
31) G. J. van Gurp: J. appl. Phys., **44** (1973) 2040.
32) E. Kovacs-Csetenyi, C. R. Vassel and I. Kovacs: Phys. Status solidi **17** (1966) K123.
33) A. P. Young, P. B. Robbins and C. M. Schwartz: *High Pressure Measurement* ed. by A. A. Giardini and E. C. Lloyd (Butterworths, Washington, 1963) p. 262.
34) I. Fujishiro, H. Mii and M. Senoo: *Les Proprietes Physiques des Solides sous Pression* (CNRS, Paris, 1970) p. 457.
35) I. Fujishiro, H. Mii, M. Senoo and I. Satoo: *Proc. 4th Inter. Conf. on High Pressure, Kyoto, 1974*, Rev. phys. Chem. Japan, Special Issue (1975) p. 240.
36) P. W. Bridgman: Proc. Am. Acad. Arts Sci., **81** (1952) 169.
37) H. J. Axon, D. Phil and W. Hume-Rothery: Proc. Roy. Soc., **A193** (1948) 1.
38) M. Senoo, H. Mii, I. Fujishiro and T. Takeuchi: Japan. J. appl. Phys., **12** (1973) 1621.
39) J. W. Kauffman and J. S. Koehler: Phys. Rev., 88 (1952) 149.
40) J. W. Kauffman and J. S. Koehler: Phys. Rev., **97** (1955) 555.
41) J. E. Bauerle and J. S. Koehler: Phys. Rev., **107** (1957) 1493.
42) R. P. Huebener: *Lattice Defects in Quenched Metals* ed. by R. M. J. Cotterill et al. (Academic Press, New York, 1964) p. 569.
43) R. M. Emrick and P. B. McArdle: Phys. Rev., 188 (1969)1156.
44) R. M. Emrick: Phys. Rev. **B6** (1972) 1144.
45) M. Charles, J. Hillairet, M. Beyeler and J. Delaplace: Phys. Rev., **B11** (1975) 4808.
46) H. Mii, I. Fujishiro and M. Kuwabara: Rep. of Toyoda Phys. Chem. Res. Inst., **19** (1966) 16 [in Japanese].
47) H. D. Stronberg and G. Jura: Science **138** (1962) 1344.

48) H. D. Stronberg and D. R. Stephens: J. Phys. Chem. Solids **25** (1964) 1015.
49) G. Jura and W. A. Stark, Jr.: Rev. sci Instrum., **40** (1969) 656.
50) H. C. Wolfe: Temperature Its Measurement and Control in Science and Industry (Reinhold, New York, 1941) p. 1312.
51) P. W. Bridgman: Proc. Amer. Acad. Arts Sci. **81** (1952) 167.
52) J. J. Jackson: *Lattice Defects in Quenched Metals* ed. by R. M. J. Cotterill et al. (Academic Press, New York, 1964) p. 467.
53) M. Senoo, H. Mii, I. Fujishiro and S. Shimizu: *17th Japan. High Pressure Conf.* (1976) 2B03 [in Japanese].
54) E. D. Whitney and R. F. Gase, Jr.: Nature **197** (1963) 1293.
55) M. Senoo, H. Mii, I. Fujishiro and T. Fujikawa: *Proc. 4th Inter. Conf. on High Pressure, Kyoto, 1974*, Rev. Phys. Chem. Japan, Special Issue (1975) p. 240.
56) M. Senoo, H. Mii, I. Fujishiro and T. Fujikawa: Japan. J. appl. Phys., **15** (1976) 871.
57) M. Senoo, H. Mii, I. Fujishiro and T. Kita: Japan. J. appl. Phys., **15** (1976) 1617.
58) P. W. Bridgman: Proc. Am. Acad. Arts Sci., **76** (1948) 55.
59) P. W. Bridgman: Proc. Am. Acad. Arts Sci., **77** (1949) 189.
60) S. N. Vaidya and G. C. Kennedy: J. Phys. Chem. Solids, **31** (1970) 2329.
61) S. N. Vaidya and I. C. Getting and G. C. Kennedy: J. Phys. Chem. Solids, **32** (1971) 2545.
62) S. N. Vaidya and G. C. Kennedy: J. Phys. Chem. Solids, **33** (1972) 1377.
63) J. C. Jamieson, A. W. Lawson and N. D. Nachtrieb: Rev. sci. Instrum., **30** (1959) 1016.
64) J. C. Jamieson, A. W. Lawson: J. appl. Phys., **33** (1962) 776.
65) M. Spieglan and J. C. Jamieson: High Temperatures High Pressures, **6** (1974) 479.
66) J. D. Barnett and H. T. Hall: Rev. sci. Instrum., **35** (1964) 175.
67) H. G. Drickamer, R. W. Lynch, R. L. Clendenen and E. A. Perez-Albuerne: *Solid State Phys.* ed. by F. Seitz and D. Turnbull (Academic Press, New York, 1966) Vol. 19, p. 135.
68) W. A. Bassett, T. Takahashi and P. W. Stook: Rev. sci. Instrum., **38** (1967) 37.
69) L. Merril. and W. A. Bassett: Rev. sci. Instrum., **45** (1974) 290.
70) M. Senoo, I. Fujishiro and H. Mii: Metal Phys. Seminar, **1** (1976) 23 [in Japanese].
71) M. Senoo. H. Mii and I. Fujishiro: J. Phys. Soc. Japan, 41 (1976) 1562.
72) K. Inoue and T. Asada: Japan. J. appl. Phys., **12** (1973) 1786.
73) J. D. Barnett, S. Block and G. J. Piermarini: Rev. sci. Instrum., 44 (1973) 1.
74) G. J. Piermarini, S. Block and J. D. Barnett: J. appl. Phys. **44** (1973) 5377.
75) A. K. Singh: Rev. sci. Instrum., **43** (1972) 1311.
76) H. Lipson and A. J. C. Wilson: J. sci. Instrum., **18** (1941) 144.
77) G. C. Kennedy and R. N. Keeler: *American Institute of Physics Handbook* 3rd ed. (McGraw-Hill, New York, 1972) p. 4-99.
78) D. L. Decker: J. Phys. Chem. Ref. Data, **1** (1972) 773.
79) R. E. Schmunk and C. S. Smith: J. Phys. Chem. Solids, **29** (1968) 541.
80) H. J. McSkimin and P. Andreatch, Jr.: J. appl. Phys., **35** (1964) 2161.
81) A. K. Singh and G. C. Kennedy: J. appl. Phys., **45** (1974) 4686.
82) B. Olinger and J. C. Jamieson: High Temperatures High Pressures, **2** (1970) 513.
83) Y. Sato, S. Akimoto and K. Inoue: High Temperatures High Pressures. **5** (1973) 289.
84) B. E. Warren: *Progress in Metal Physics* ed. by B. Chalmers and R. King (Pergamon Press, New York, 1959) Vol. 8, p. 147.
85) A. J. Goldman and C. N. J. Wagner: Acta metallurgica **11** (1963) 405.
86) M. S. Paterson: J. appl. Phys., **23** (1952) 805.
87) B. E. Warren and E. P. Warekois: Acta metallurgica, **3** (1955) 473.
88) F. J. Bradshaw and Pearson: Phil. Mag., **1** (1956) 812.
89) A. Ascoli, M. Asdente, M. Germagoli and A. Manara: J. Phys. Chem. Solids **6** (1958) 59.
90) G. L. Bacchella, E. Germagnoli and S. Granata: J. appl. Phys., **30** (1959) 748.
91) H. Mii, I. Fujishiro, M. Senoo and T. Morishita: Rep. of Toyoda Phys. Chem. Res. Inst. **24** (1971) 46 [in Japanese].
92) H. Mii, I. Fujishiro, M. Senoo and K. Narumi: Rep. of Toyoda Phys. Chem. Res. Inst., **29** (1976) 1 [in Japanese].